Title page

Title: Tension stiffening of rebar-reinforced coarse aggregate ultra-high performance concrete (R-CA-UHPC): Tension capacity prediction and crack width calculation

Author names: Zhanchong Shi[a,b,c], Chen Lin[b,d], Qingtian Su[a,e,*], Terje Kanstad[b], Liberato Ferrara[c]

Affiliations: [a]Department of Bridge Engineering, Tongji University, Shanghai 200092, China;

[b]Department of Structural Engineering, Norwegian University of Science and Technology, Richard Birkelandsvei 1A, 7034 Trondheim, Norway;

[c]Department of Civil and Environmental Engineering, Politecnico di Milano, Piazza Leonardo DaVinci 32, 20133 Milan, Italy;

[d]Department of Civil Engineering and Smart Cities, Shantou University, Shantou 515063, China;

[e]Shanghai Engineering Research Center of High Performance Composite Bridges, Shanghai 200092, China.

Corresponding author: Qingtian Su (E-mail: sqt@tongji.edu.cn)

Address: 1239 Siping Road**,** Tongji University, Shanghai 200092, China.

Tension stiffening of rebar-reinforced coarse aggregate ultra-high performance concrete (R-CA-UHPC): Tension capacity prediction and crack width calculation

Zhanchong Shi[a,b,c], Chen Lin[b,d], Qingtian Su[a,e,*], Terje Kanstad[b], Liberato Ferrara[c]

[a]*Department of Bridge Engineering, Tongji University, Shanghai 200092, China*

[b]*Department of Structural Engineering, Norwegian University of Science and Technology, Richard Birkelandsvei 1A, 7034 Trondheim, Norway*

[c]*Department of Civil and Environmental Engineering, Politecnico di Milano, Piazza Leonardo DaVinci 32, 20133 Milan, Italy*

[d]*Department of Civil Engineering and Smart Cities, Shantou University, Shantou 515063, China*

[e]*Shanghai Engineering Research Center of High Performance Composite Bridges, Shanghai 200092, China*

ABSTRACT

Coarse aggregate ultra-high performance concrete (CA-UHPC) requires characteristic tensile properties for structural design practices both in the serviceability and ultimate limit states (SLS and ULS). Through uniaxial tension testing, this study aims to identify the post-cracking performance of rebar-reinforced CA-UHPC (R-CA-UHPC), including cracking, tension stiffening, and tension capacity. Utilizing experimental data derived from average tensile responses, a tension-stiffening model of cracked CA-UHPC was developed, considering scenarios with and without the shrinkage effect. The findings demonstrate that the restrained shrinkage effect significantly influences the tension-stiffening of cracked CA-UHPC in the pre-yielding phase, while becoming negligible for the post-yielding behavior. The shrinkage-corrected model exhibits reinforcement ratio independence. Furthermore, the non-shrinkage-corrected model demonstrates superior predictive accuracy of

R-CA-UHPC's global tensile response compared to the CA-UHPC tensile constitutive model. Subsequently, a tension-stiffening-based approach was derived and validated to calculate crack widths in rebar-reinforced UHPC members.

Keywords: CA-UHPC, tension stiffening, cracking, restrained shrinkage effect, crack width calculation.

1. Introduction

Tension stiffening represents the ability of concrete to carry tension between cracks in a rebar-reinforced concrete (RC) member, which helps control member stiffness, deformation, and crack widths related to satisfying serviceability requirements [1]. While plain concrete is assumed to carry tension between the cracks only, fiber-reinforced concrete (FRC) is able to carry significant tensile stresses across a crack in addition to between the cracks [2–5]. Additionally, rebar-reinforced FRC (R-FRC) members exhibit tension stiffening both in the pre- and post-yielding range, contrast to normal rebar-reinforced concrete (R-NC) members where tension stiffening disappears after rebar yielding[3]. Understanding the tension stiffening effects enables the development of average tensile stress-strain relationships and models that can predict RC member post-cracking response using smeared-crack finite element and layered beam section models [6–8].

Ultra-high performance concrete (UHPC), as a new generation of FRC, is mainly characterized by(1) a compressive strength greater than 120 MPa; (2) a disconnected pore structure that significantly reduces permeability and thus enhances durability; and (3) sufficient fiber reinforcement to allow for sustained post-cracking tensile resistance that exceeds a minimum cracking strength of 5 MPa [9]. However, a low water-to-binder ratio (less than 0.2) and high dosage of binders result into high autogenous shrinkage at early ages[10], increasing the cracking risk for UHPC structures. Addressing this issue, coarse aggregate ultra-high performance concrete (CA-UHPC) was proposed by adding coarse

aggregates to partially replace the fine fractions in UHPC[11]. One consequence is higher compressive strength and elastic modulus compared with conventional UHPC[12]. Due to these advantages, CA-UHPC has been widely used in large structural applications, including e.g., the concrete bridge deck in the Fifth Nanjing Yangtze River Bridge in China [12], a 2×600 m cable-stayed bridge.

Research on tension stiffening in rebar-reinforced UHPC (R-UHPC) members remains limited [13–20], with previous studies focusing solely on UHPC without coarse aggregates. While Yuan [13] and Hung et al [15] have developed tension-stiffening models for cracked UHPC, the addition of coarse aggregate in CA-UHPC potentially reduces tensile performance compared to conventional UHPC. This necessitates developing and validating a specific tension-stiffening model for predicting mechanical behavior in cracked rebar-reinforced coarse aggregate UHPC (R-CA-UHPC) elements. Additionally, proper assessment of shrinkage effects is crucial, as studies by Fields et al.[21] and Yuan[13] show that UHPC's significant shrinkage can reduce tension stiffening in cracked elements, with higher reinforcement ratios leading to greater performance reduction.

Cracking might critically affect RC structures by reducing cross-sectional and structural stiffness, leading to increased deformation and compromised serviceability[22]. Additionally, excessive cracking may induce reinforcement corrosion under aggressive environmental conditions, reducing the load-bearing capacity and service life. Thus, cracking control and accurate crack width prediction are essential for both serviceability and ultimate limit state verification. Current design codes inadequately address crack width calculation for R-UHPC structures. While the French code NF P 18-710[23] exempts significant strain hardening UHPC (class T3) structures from crack control and provides calculation methods for strain softening (class T1) and limited strain hardening UHPC (class T2), the Japanese recommendation[24] conservatively limits UHPC tensile stress to first cracking strength,

potentially underutilizing UHPC's exceptional tensile performance.

Leutbecher et al.[25] proposed a crack width calculation method for R-UHPC structures incorporating steel fiber contribution, though it requires experimental determination or literature-based assumptions of fiber/matrix bond strength. While Luo et al.[26] and Qiu[27] proposed calculation methods for crack widths in R-UHPC and steel-UHPC composite flexural members, their iterative neutral axis calculations seem too complex for practical design applications. Currently, research on R-UHPC crack width calculation remains insufficient, necessitating development of a method that both accounts for UHPC's superior tensile strength and rebar/UHPC interface bond properties while maintaining practical simplicity.

Based on the research gaps described above, this study aims to identify tension stiffening in R-CA-UHPC to establish methods for post-cracking tension capacity prediction and crack width calculation, encompassing both ultimate and serviceability limit states. Through uniaxial tension tests on R-CA-UHPC specimens previously reported in [28], tension stiffening models were developed. Also, the influence of the restrained shrinkage effect on tension stiffening was quantified. Subsequently, the tension capacity was analytically determined, and a novel tension-stiffening-based methodology for crack width calculation in R-UHPC structural members was developed and validated.

2. Tension stiffening

2.1 Uniaxial tension test

2.1.1 Materials and methods

To identify the tension stiffening of R-CA-UHPC, the uniaxial tension test data obtained by Shi et al.[28] was used. In these experiments, dog-bone-shaped specimens, with a length of 560 mm, a central cross section of 50 mm×100 mm, and an end section of 100 mm×100 mm, were designed, as shown in Fig.1. The investigated rebar configurations were: (1) rebar

diameters d_s, equal to 10 mm, 12 mm, 14 mm, and 16mm (section with single rebar); (2) rebar quantities with one, two and three 10-mm-diameter rebars. The specimens are summarized in Table 1, and each set had four identical samples. Fig.1(f) presents the uniaxial tension test setup, where two extensometers with gauge length 200 mm were attached to the central part of the specimens to capture the extension. It is noted that the R-CA-UHPC specimens were placed in a curing room with a temperature of 20±2°C and relative humidity of 95% for 28 days before tension testing.

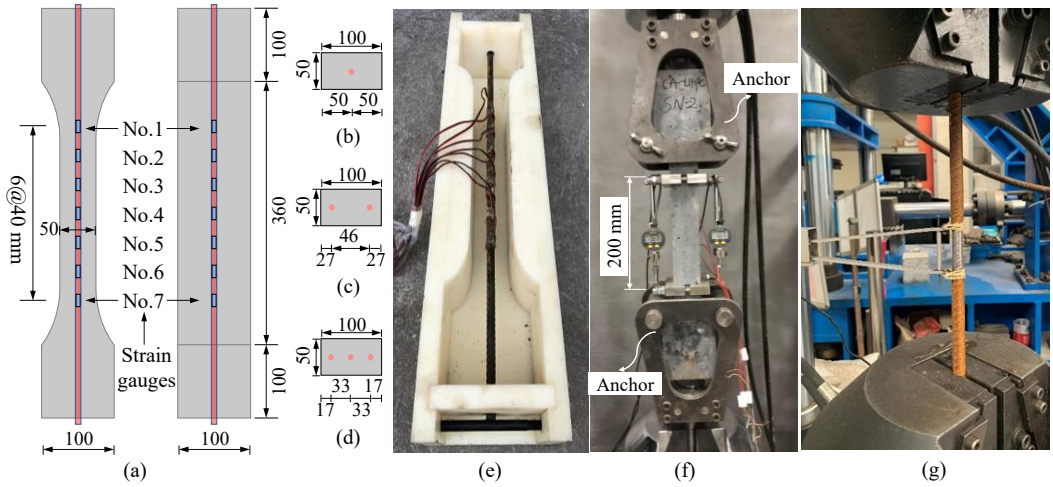

Fig. 1. Samples and test setup (unit: mm) [28]: (a) sample size; (b) one-rebar section; (c) two-rebars section; (d) three-rebars section; (e) casting mold; (f) uniaxial tension test setup for R-CA-UHPC; and (g) uniaxial tension test setup for rebar.

Table 1. R-CA-UHPC specimen details.

No.	Rebar configuration	Reinforcement ratio ρ_s
SN-1~SN-4	d_s10	1.6%
SN-1~SN-4	2d_s10	3.2%
SN-1~SN-4	3d_s10	5.0%
SN-1~SN-4	d_s12	2.3%
SN-1~SN-4	d_s14	3.2%
SN-1~SN-4	d_s16	4.2%

The CA-UHPC [28] adopted was made of 1173 kg/m^3 reactive powder, 616 kg/m^3 sand, 472 kg/m^3 basalt aggregate, 198 kg/m^3 steel fibers, 25.7 kg/m^3 superplasticizer, and 138 kg/m^3

water. Fig.2(a) shows the applied tensile constitutive model，while the characteristic parameters are listed in Table 2. The material exhibits strain softening after the first crack [29]. Steel rebars of quality HRB400 were used [28]. Uniaxial tensile tests，as shown in Fig.1(g)，were conducted to determine the complete tensile stress-strain responses for the rebars as well as the simplified tensile constitutive law presented in Fig.2(b) with mechanical properties summarized in Table 3.

Table 2. Basic mechanical properties of concrete [28].

Concrete	E_c [MPa]	f_c [MPa]	f_{ct} [MPa]	f_{ctr} [MPa]	ε_{ctr} [$\times10^{-6}$]	$\varepsilon_{ct,max}$ [$\times10^{-6}$]
CA-UHPC	52000±6538	128±10	7.83±0.78	6.47±0.84	2500	32500

Notes: E_c and f_c denote elastic modulus and compressive strength, respectively. f_{ct}, f_{ctr}, ε_{ctr}, and $\varepsilon_{ct,max}$ are the tensile strength, post-peak residual tensile strength, post-peak residual tensile strain, and maximum tensile strain, respectively.

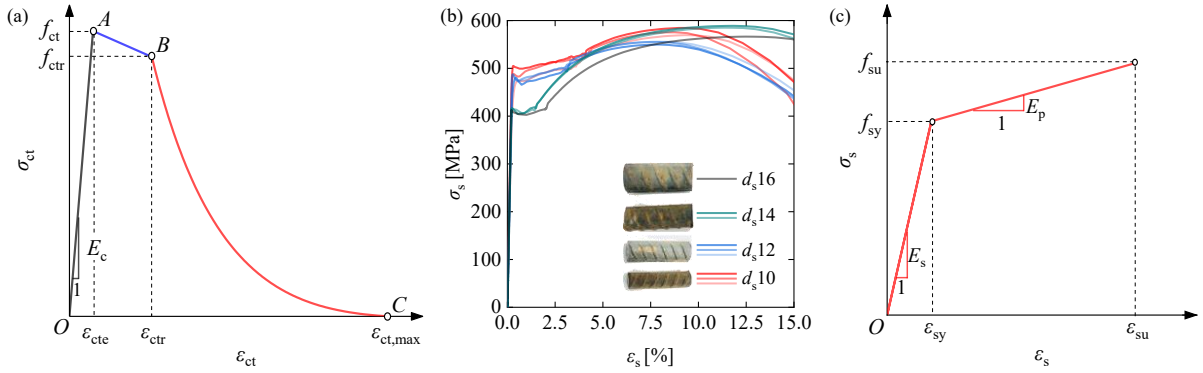

Fig. 2. Axial tensile constitutive models: (a) of CA-UHPC [29]; (b) tensile stress-strain response of rebar; and (c) simplified tension constitutive model of rebar (based on and adapted from [28]).

Table 3. Mechanical properties of the bilinear constitutive model of the steel rebar [28].

d_s [mm]	f_{sy} [MPa]	f_{su} [MPa]	ε_{sy} [$\times10^{-6}$]	ε_{su} [$\times10^{-6}$]	E_s [MPa]	E_p [MPa]
10	488	577	2438	90042	200187	1010
12	470	554	2382	77811	197439	1103
14	406	587	2104	116164	192978	1587
16	407	566	1958	124925	207880	1296

Notes: f_{sy}, f_{su}, ε_{sy}, ε_{su}, E_s, and E_p denote the yielding strength, tensile strength, yielding strain, tensile strain at the tensile strength, elastic modulus, and plastic modulus, respectively.

2.1.2 Test results

Fig.3 shows the axial load versus the average member strain of the test specimens. The tension response is composed of three distinct stages [28]: Phase I, the elastic uncracked stage. Phase II, cracking stage, from first cracking to yielding of the steel rebar. Phase III, post-yielding stage. The specimens were exposed to shrinkage occurring before the load test. Crack localization appears after rebar yielding, and no or negligible amount of splitting cracks develop. The tensile capacity of R-CA-UHPC is significantly larger than that of the bare rebar even after yielding, differing from R-NC, for which the tensile capacity is approximately the same as the bare rebar[21]. Fig.4 illustrates the crack development process and the final rebar fracture (denoted as phase IV) for R-CA-UHPC members under direct tension.

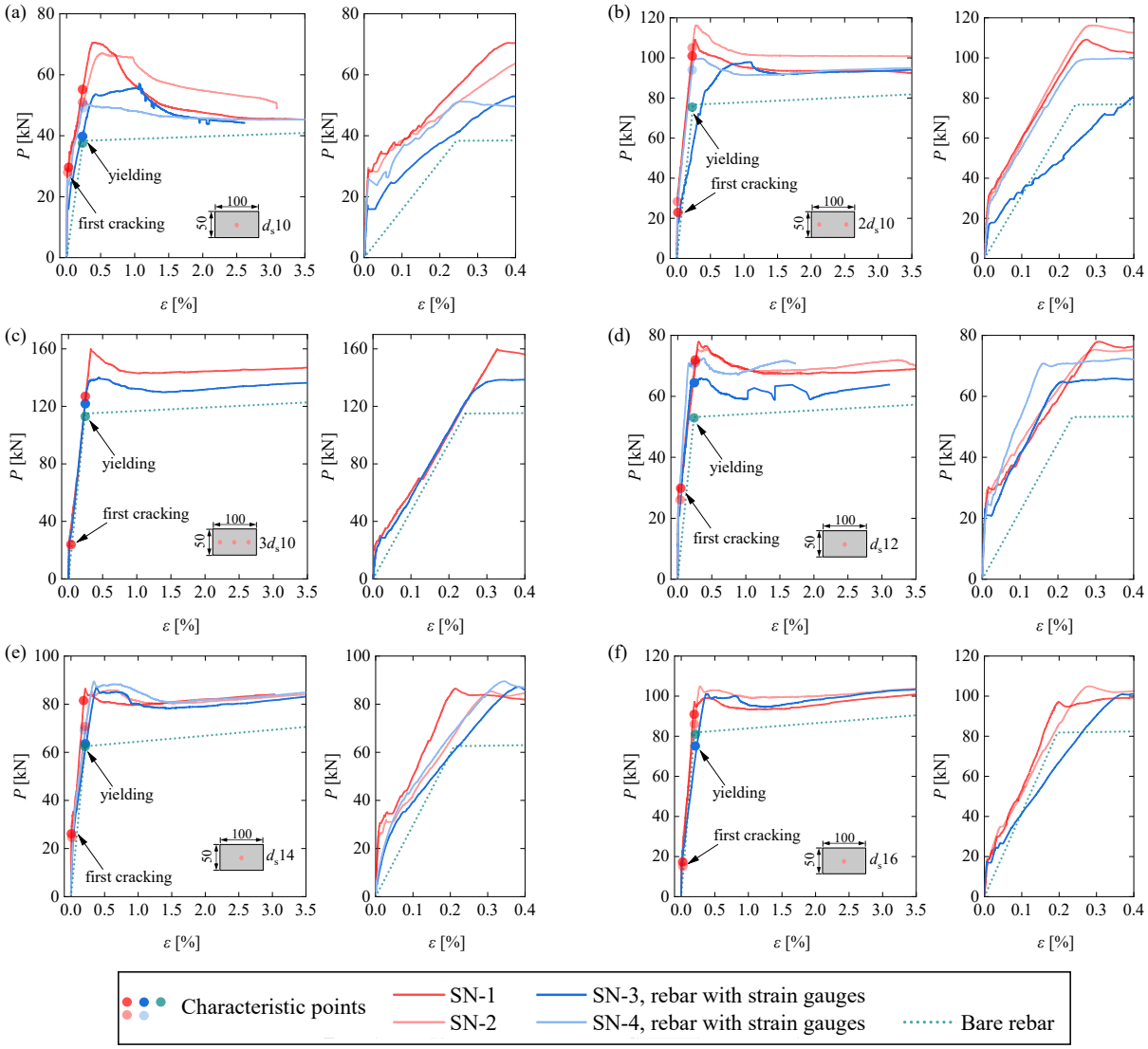

Fig. 3. Axial load-average member strain response of R-CA-UHPC: (a) d_s10; (b) $2d_s10$; (c) $3d_s10$; (d) d_s12; (e) d_s14; and (f) d_s16 (based on and adapted from [28]).

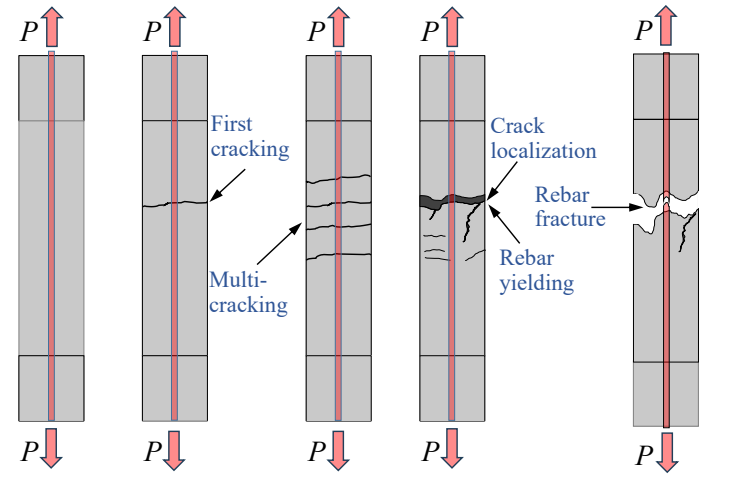

Fig. 4. Crack development of R-CA-UHPC.

2.2 Tension stiffening modelling

2.2.1 Tension stiffening

Fig.5 shows the typical uniaxial tension response of RC members, including R-NC and R-CA-UHPC, where tension stiffening is assumed to be the difference between the member response and the bare rebar response[21]. The member response can be divided into three distinct phases defined by the first cracking point A (ε_{cr}, P_{cr}) and the yielding point B (ε_y, P_y): the linear-elastic, the crack development, and the post-yielding stages. More precisely, tension stiffening is defined to represent the concrete contribution to the tension capacity of the RC member after first cracking.

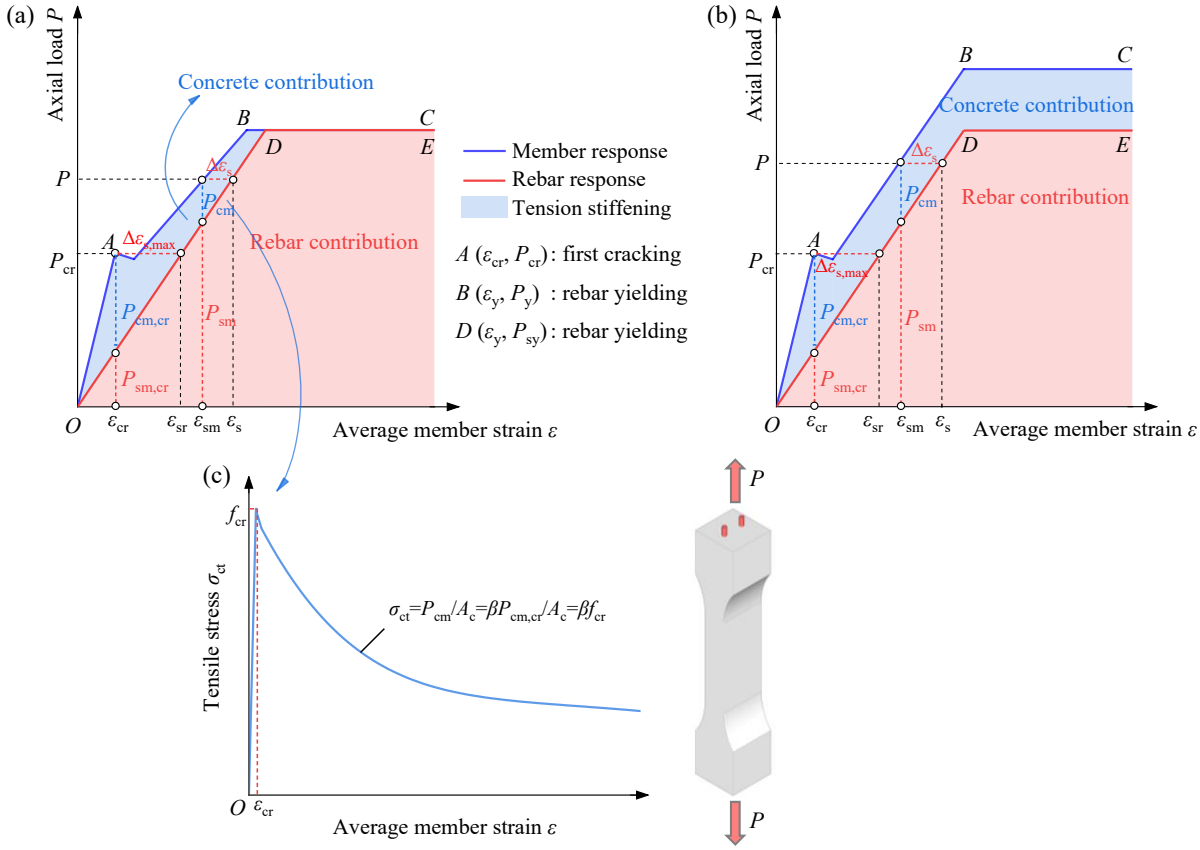

155

156 **Fig. 5.** Schematic axial tension response of RC members: (a) R-NC; (b) R-CA-UHPC; and (c)

157 tension-stiffening model of cracked concrete.

158 When normal concrete cracks, the concrete at the crack fails to carry tension, but the

159 tensile force is still transferred to the neighboring solid concrete from the rebar through the

160 interface bond[21]. Hence, the stresses in the concrete vary between the cracks along the

161 member length, resulting in an average concrete tensile stress lower than the tensile strength

162 f_{cr}, shown in Fig.5(c). For R-CA-UHPC, apart from the bond-transferring mechanism,

163 concrete at the crack continues to carry tension due to the post-cracking strength resulting

164 from the fiber-bridging. More cracks appear with increasing external load, while the average

165 tensile stress in concrete continues to decrease.

166 When crack spacing has stabilized, and no more transverse cracks develop, the observed

167 decrease in average concrete stress and tension stiffening continues but at a slower rate,

168 mainly due to the loss of bond from internal cracking and slip between the two materials [30].

Tension stiffening drops to zero at yielding because the rebar is not able to transfer tensile forces larger than the yield force across cracks, as shown in Fig.5(a). By comparison, the tension stiffening of R-CA-UHPC continues even after yielding of the rebars, as shown in Fig.5(b), due to the fiber-bridging effect and the enhanced interface bond properties, as demonstrated from the cracking patterns with no obvious splitting cracks observed.

There are two methods for characterizing the tensile stiffness[21], one is the tension-stiffening strain approach, and the other one is the load-sharing approach. According to the strain approach, as shown in Fig.5, for any given external load P, the average member strain after concrete cracking is ε_{m}, which is the same as the average strain of the rebar $\varepsilon_{\mathrm{sm}}$. The strain of the bare rebar under the same load P is marked as ε_{s}. The tension-stiffening strain $\Delta\varepsilon_{\mathrm{s}}$ is thus the difference between $\varepsilon_{\mathrm{sm}}$ and ε_{s}. Accordingly, $\varepsilon_{\mathrm{sm}}$ can be expressed as:

$$\varepsilon_{\mathrm{sm}} = \varepsilon_{\mathrm{s}} - \Delta\varepsilon_{\mathrm{s}} = \varepsilon_{\mathrm{s}} - \beta\Delta\varepsilon_{\mathrm{s,max}} \qquad \beta = \frac{\Delta\varepsilon_{\mathrm{s}}}{\Delta\varepsilon_{\mathrm{s,max}}} \tag{1}$$

where β is termed the bond factor; $\Delta\varepsilon_{\mathrm{s,max}}$ is the tension-stiffening strain at first cracking, $\Delta\varepsilon_{\mathrm{s,max}}=\varepsilon_{\mathrm{sr}}-\varepsilon_{\mathrm{cr}}$; $\varepsilon_{\mathrm{sr}}$ and $\varepsilon_{\mathrm{cr}}$ are the strain of the bare rebar and the member at first cracking, respectively.

According to the load-sharing approach[1], the axial member load P is shared by the rebar P_{sm} and the concrete P_{cm}, with P_{cm} is given as：

$$P_{\mathrm{cm}} = P - P_{\mathrm{sm}} \tag{2}$$

The average concrete stress can be expressed by:

$$\sigma_{\mathrm{ct}} = \frac{P_{\mathrm{cm}}}{A_{\mathrm{c}}} \tag{3}$$

where A_{c} is the effective area of concrete in tension.

The tensile load shared by rebar and concrete at first cracking can be marked as $P_{\mathrm{sm,cr}}$ and $P_{\mathrm{cm,cr}}$, respectively. Consequently, the first cracking strength of concrete is given as:

$$f_{cr} = \frac{P_{cm,cr}}{A_c} \tag{4}$$

The load-sharing-approach-based tension-stiffening bond factor β is expressed as:

$$\beta = \frac{P_{cm}}{P_{cm,cr}} = \frac{\sigma_{ct}}{f_{cr}} \tag{5}$$

The bond factors β obtained according to Eq.(1) and Eq.(5) are identical. The relation between the tension-stiffening strain of the rebar $\Delta\varepsilon_s$ and the tension-stiffening stress of the concrete βf_{cr} is plotted in Fig.5(a), and is given as:

$$E_s A_s \Delta\varepsilon_s = \beta A_c f_{cr} \tag{6}$$

The average tensile stress-strain curve of the cracked structural member obtained by the load-sharing approach is named as the tension-stiffening model (TSM). The bond factor β obtained is regarded as a normalized material characteristic of cracked concrete[21].

2.2.2 Restrained shrinkage effect

In RC members the free shrinkage of concrete is restrained by rebars, thus inducing tensile strains and stresses in concrete and corresponding compressive strains and stresses in the rebars. The schematic diagram [31]of this restrained shrinkage effect is shown in Fig.6(a), in which ε_{cs} is the free shrinkage strain of concrete; $\varepsilon_{cs,re}$ is the restrained shrinkage strain, i.e., the developed shrinkage of concrete under the constraint of the rebar; $\varepsilon_{ct,re}$ is the induced restrained tensile strain in concrete, corresponding to the restrained tensile stress $\sigma_{ct,re}$. Relevant studies [13,21] have revealed that neglecting the restrained shrinkage effect can lead to incorrect estimation of the stresses in rebars and concrete, thus underestimating the tension stiffening, and that the impact increases with the increase of reinforcement ratio as well as free shrinkage of concrete.

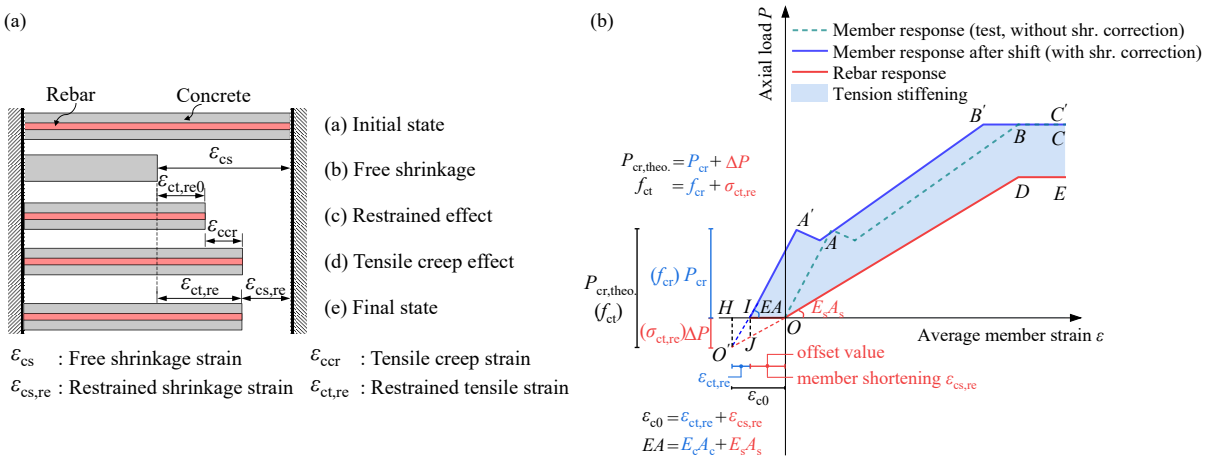

Fig. 6. Restrained shrinkage effect: (a) schematic diagram [31]; and (b) influence on tension stiffening.

As plotted in Fig.6(b), the member response compensated for the restrained shrinkage effect (curve IA′B′C′) was obtained by shifting the experimental member response (curve OABC) to the left by the initial member shortening $\varepsilon_{cs,re}$. For convenience, the two member responses before and after shifting were marked as without/with shrinkage correction. From the member response with shrinkage correction, it is obvious that only concrete sustains tension when the average member strain is lower than the restrained shrinkage strain $\varepsilon_{cs,re}$. The difference between the corrected member response and the bare rebar response is the actual tensile contribution of concrete. It shows that ignoring the restrained shrinkage effect in the experiment will underestimate the tensile contribution of concrete to the member.

In addition, the difference in the vertical coordinates between point O′ and point I is the difference between the theoretical first cracking load $P_{cr,theo}$ (corresponding to the tensile strength of concrete f_{ct}) and the experimental first cracking load P_{cr} (corresponding to the first cracking stress f_{cr}). The difference in the horizontal coordinates is the restrained tensile strain $\varepsilon_{ct,re}$ in concrete. Considering that the point O′ is obtained by two elastic curves, where the elastic modulus of concrete is a constant, $\varepsilon_{ct,re}=\sigma_{ct,re}/E_c$ and $\varepsilon_{c0}=\Delta P/E_sA_s=\varepsilon_{ct,re}+\varepsilon_{cs,re}$ may be obtained. It should be noted that ε_{c0} obtained through this elastic method is not equal to the

free shrinkage of concrete ε_{cs}.

The measured axial load-average member strain response of R-CA-UHPC after shrinkage correction is shown in Fig.7, where the restrained shrinkage strain $\varepsilon_{cs,re}$ is calculated according to the first author's previous work [28], as expressed in Eq.(7).

$$\varepsilon_{cs,re} = \varepsilon_{cs}\left(0.973 - 1.91\alpha_E\rho_s\right) \tag{7}$$

where: ε_{cs} is the free shrinkage of CA-UHPC, equal to 673 $\mu\varepsilon$ [28]; α_E is the elastic modulus ratio of rebar to CA-UHPC; while ρ_s is the reinforcement ratio.

According to the load-sharing approach, the average tensile stress-strain responses for cracked CA-UHPC with and without shrinkage correction are compared in Fig.8. As shown, there are two pronounced features for the average tensile stress-strain curve without shrinkage correction. One is that the first cracking strength, which is significantly lower than the measured tensile strength of CA-UHPC (7.83 MPa), and this effect increases with the increase of reinforcement ratio. Secondly, the softening branch exhibits a sharp rise after reaching the yielding strain (approximately 0.2%), indicating an increase in the tensile contribution of CA-UHPC, which is inconsistent with the crack localization in CA-UHPC. These phenomena can be explained by the restrained shrinkage effect.

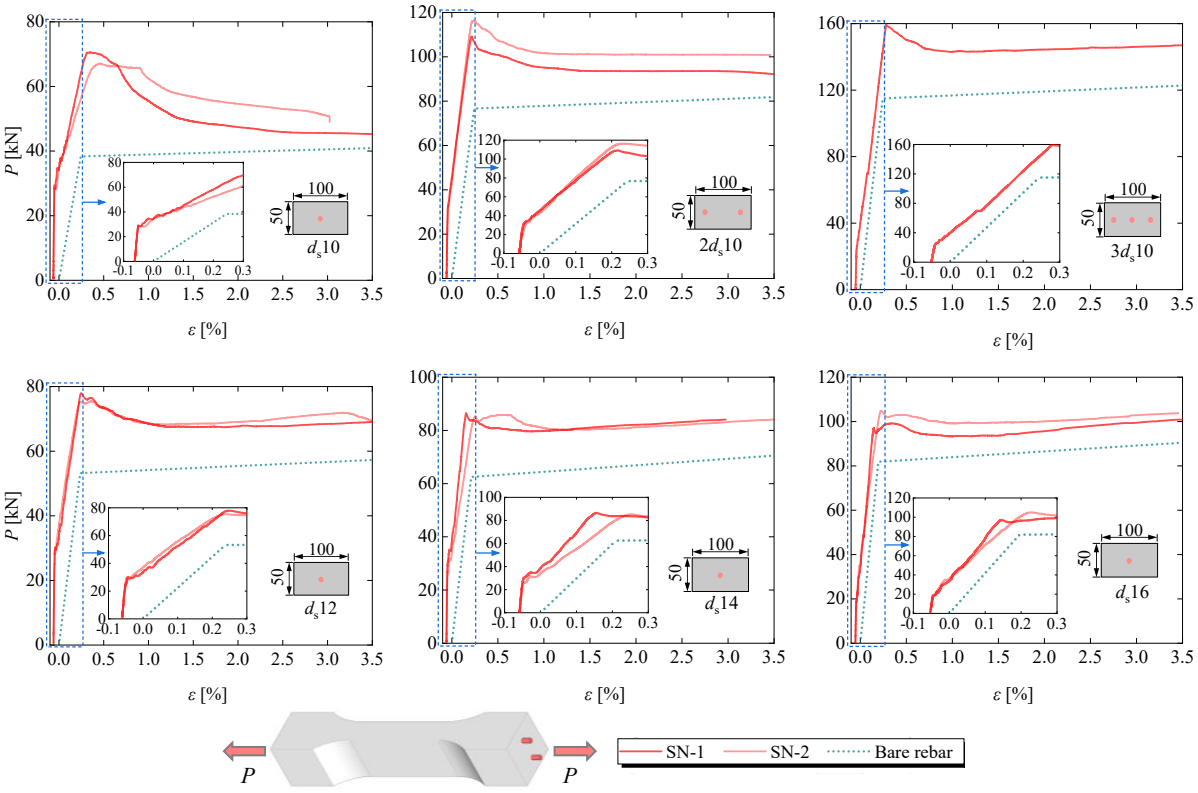

Fig. 7. Axial load-average member strain response with shrinkage correction for R-CA-UHPC.

By comparison, the first cracking stress of the average tensile stress-strain curve with shrinkage correction is close to the tensile strength of CA-UHPC. And the softening branch presents a smoother and continuous downward trend, which is similar to the softening branch of the tensile constitutive model of CA-UHPC. It indicates that considering the shrinkage correction can provide a more accurate evaluation of the tensile contribution of concrete to the member. Moreover, the difference between the average tensile stress-strain curves with and without shrinkage correction is more significant from the first cracking point to the yielding point, while the difference after yielding can be neglected. This is because the fiber/matrix interface debonding at the localized crack is the main contribution to tension stiffening at the post-yielding stage.

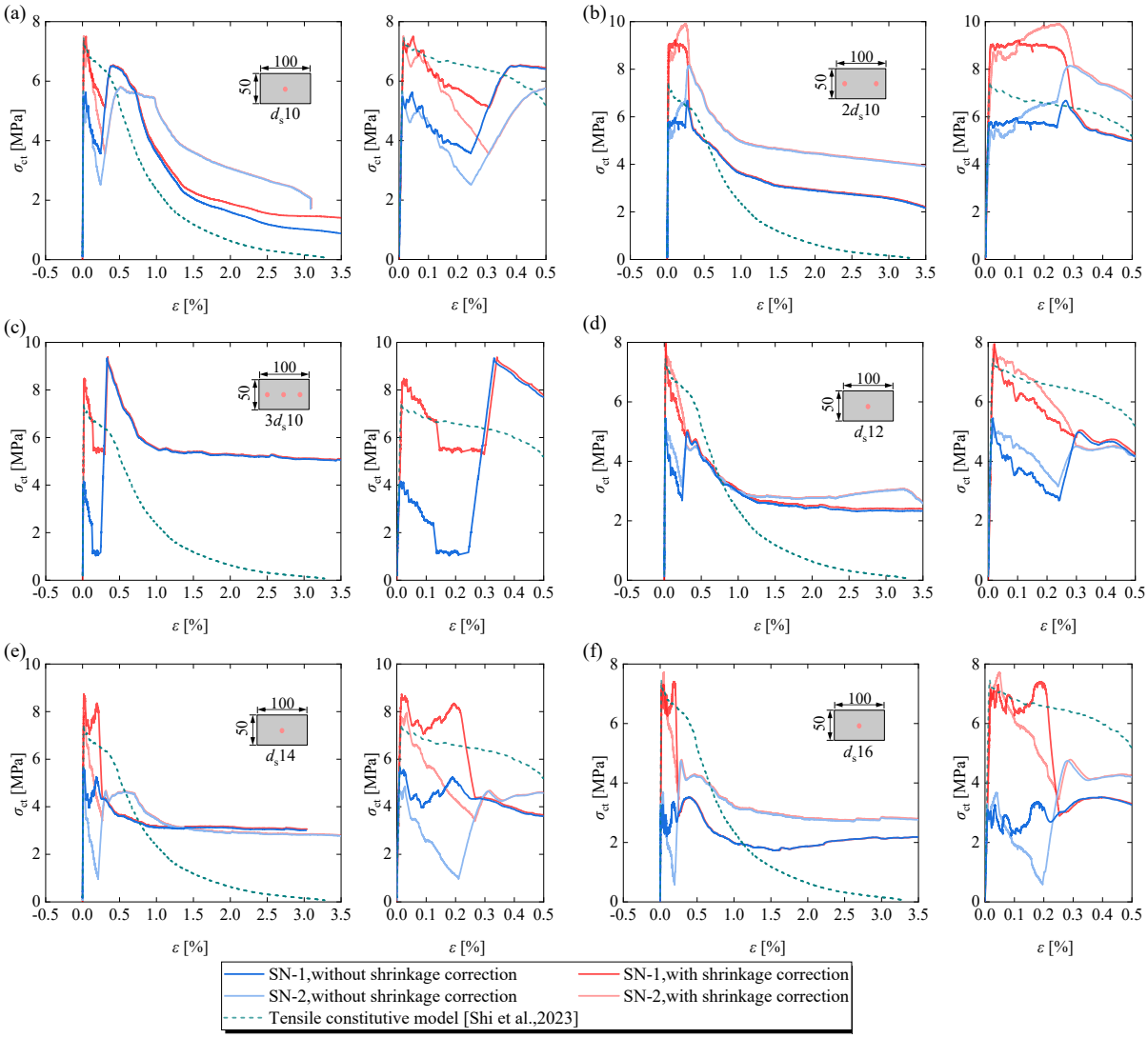

Fig. 8. Average tensile stress-strain response for cracked CA-UHPC: (a) d_s10; (b) 2d_s10; (c) 3d_s10; (d) d_s12; (e) d_s14; and (f) d_s16.

A comparison of the average tensile stress-strain responses for cracked CA-UHPC corresponding to different reinforcement ratios is shown in Fig.9. As shown, the curves with shrinkage correction show better mutual agreement than those without. The consequence is that the average tensile stress-strain relation for cracked CA-UHPC is independent of reinforcement ratios as long as the restrained shrinkage is included in the analysis of the member response.

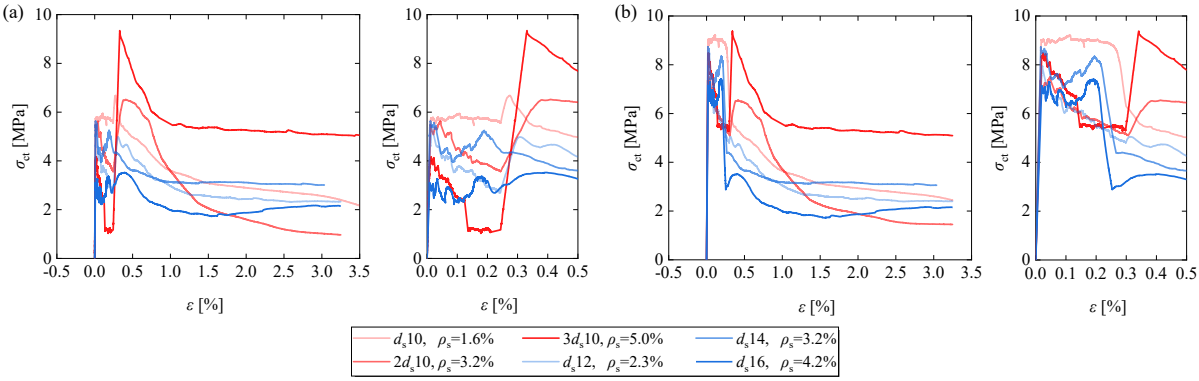

Fig. 9. Comparison of average tensile stress-strain responses for cracked CA-UHPC: (a) without shrinkage correction; and (b) with shrinkage correction.

2.2.3 Tension stiffening model

Fig.10 presents the tension-stiffening stress-strain curves with and without shrinkage correction for the R-CA-UHPC, and the normalized tension stiffening model (TSM) is fitted to the experiments using the exponential function below:

$$\beta = \frac{\sigma_{ct}}{f_{cr}} = \left[1 + \left(a\frac{\varepsilon_{ct}-\varepsilon_{cr}}{\varepsilon_{ct,max}-\varepsilon_{cr}}\right)^3\right] e^{-b\frac{\varepsilon_{ct}-\varepsilon_{cr}}{\varepsilon_{ct,max}-\varepsilon_{cr}}} \tag{8}$$

where: β is the bond factor; f_{cr} and ε_{cr} are the first cracking strength and strain, respectively; ε_{ct} is any tensile strain, representing the average member strain; $\varepsilon_{ct,max}$ is the maximum average member strain, taken as 3.25% (corresponding to an elongation of 6.5 mm over the gauge length of 200 mm); while a and b are model parameters to be fitted.

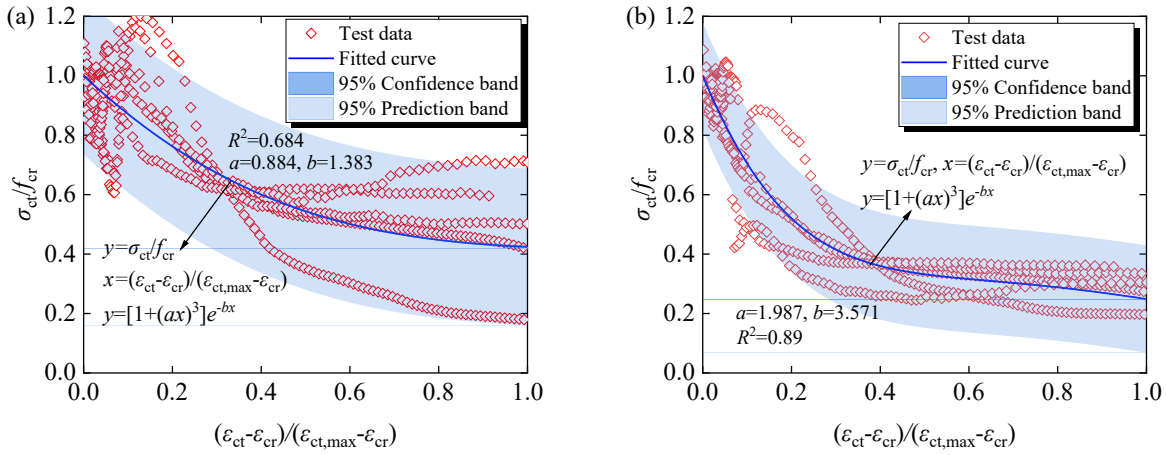

Fig. 10. Normalized tension-stiffness stress-strain fitting curve: (a) without shrinkage correction; and (b) with shrinkage correction.

The fitted results are shown in Fig.10, while the model parameters are listed in Table 4. The goodness-of-fit R^2 with shrinkage correction is 0.890, far superior to that without shrinkage correction which is 0.684. This is because the normalized fitting method is based on the first cracking strength, which is substantially influenced by the restrained shrinkage effect. It is noted that the formulated model is suitable for CA-UHPC with a steel fiber volume fraction of 2.5%, and R-CA-UHPC with a reinforcement ratio within 5%.

Table 4. Fitted parameters of normalized tension-stiffening stress-strain curve.

Types	a	b	R^2
without shrinkage correction	0.884	1.383	0.684
with shrinkage correction	1.987	3.571	0.890

A comparison of bond factor β based on the tension constitutive model (TCM) and the tension-stiffening model (TSM) is shown in Fig.11(a). It is clear that the TSM curve lies above the TCM. As β of TCM drops to zero, the β of TSM is still greater than 0.25. Although both curves present a softening response, the underlying mechanisms are fundamentally different. The softening branch of the tension constitutive model is essentially a strain-softening behavior, reflecting the development of stress-strain after the occurrence of crack localization in plain concrete. Tension stiffening only develops in RC and originates predominately from the tensile capacity of concrete between cracks[1], being affected by the transfer of tensile force from rebar to concrete through the interface bond. For fiber-reinforced concrete, such as CA-UHPC, tension stiffening as considered in this research also includes the residual tensile bearing capacity contributed by the fiber-bridging effect at cracks[3,5].

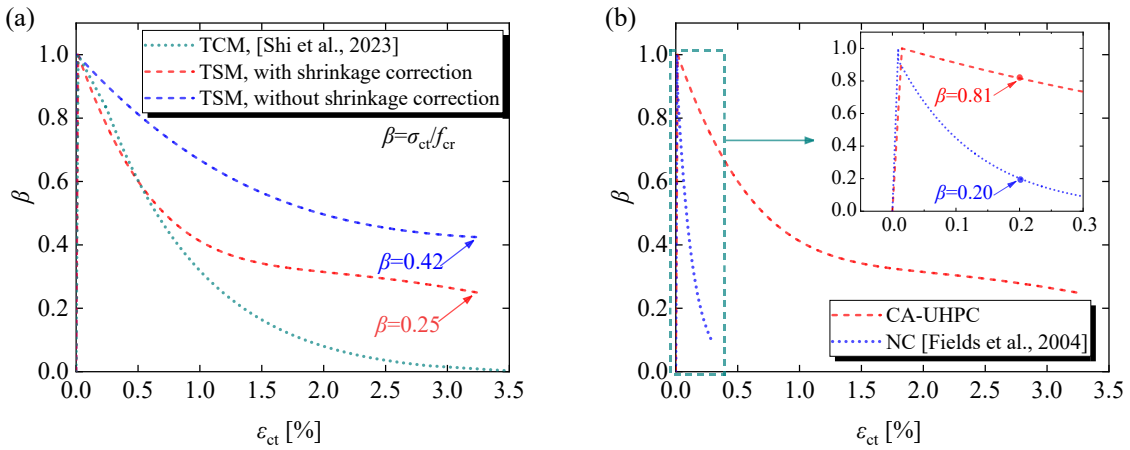

Fig. 11. Comparison of bond factor β: (a) different models; and (b) different concretes.

The bond factors β of CA-UHPC and NC are compared in Fig.11(b), where bond factors were developed by considering shrinkage correction. It is observed that the bond factor of CA-UHPC is significantly greater than that of NC. The bond factor of CA-UHPC is 0.81, which is 4 times the NC one, at the yielding strain (approximately 0.2%). When the bond factor of NC falls to zero, the corresponding item of CA-UHPC remains greater than 0.2. The mechanism behind this phenomenon is the improved tensile strength, the enhanced interface bond properties, and the bridging effect for CA-UHPC, which will be further quantified in the following section.

The exponential tension-stiffening model was further simplified into the bilinear form for the convenience of application, as shown in Fig.12. Considering the elastic-linear ascending branch simultaneously, the simplified tension-stiffening model of cracked CA-UHPC can be expressed as:

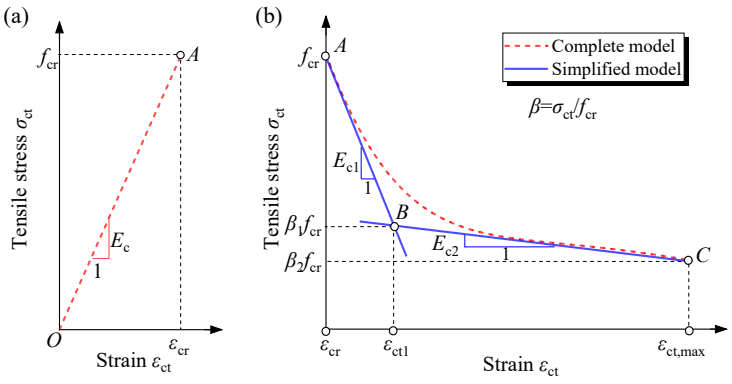

Fig. 12. Tension-stiffening model of cracked CA-UHPC: (a) ascending branch; and (b) softening branch.

$$\sigma_{ct}=\begin{cases}E_c\varepsilon_{ct} & 0\le\varepsilon_{ct}\le\varepsilon_{cr}\\ f_{cr}-E_{c1}\left(\varepsilon_{ct}-\varepsilon_{cr}\right) & \varepsilon_{cr}<\varepsilon_{ct}\le\varepsilon_{ct1}\\ \beta_1 f_{cr}-E_{c2}\left(\varepsilon_{ct}-\varepsilon_{ct1}\right) & \varepsilon_{ct1}<\varepsilon_{ct}\le\varepsilon_{ct,max}\end{cases} \tag{9}$$

The parameters shown in Fig.12 and Eq.(9) are summarized in Table 5, where β_1 and β_2 are characteristic coefficients, $E_{c1}=(f_{cr}-\beta_1 f_{cr})/(\varepsilon_{ct1}-\varepsilon_{cr})$, $E_{c2}=(\beta_1 f_{cr}-\beta_2 f_{cr})/(\varepsilon_{ct,max}-\varepsilon_{ct1})$. The first cracking strength f_{cr} with shrinkage correction corresponds to the tensile strength f_{ct} of CA-UHPC. While the first cracking strength f_{cr} without shrinkage correction, is calculated according to the first author's previous work [28], as expressed in Eq.(10).

$$f_{cr}=f_{ct}(1-\zeta) \tag{10}$$

where: ζ is the restrained degree, reflecting the restrained shrinkage effect, and is predicted according to Eq.(11)[28].

$$\zeta=0.045+2.83\alpha_E\rho_s \tag{11}$$

where α_E is the elastic modulus ratio of rebar to CA-UHPC, ρ_s is the reinforcement ratio.

Table 5. Parameters of the simplified tension-stiffening model of CA-UHPC.

Types	Point A		Point B		Point C	
	f_{cr}	ε_{cr}	β_1	ε_{ct1} [$\times10^{-6}$]	β_2	$\varepsilon_{ct,max}$ [$\times10^{-6}$]
without shrinkage correction	$f_{ct}(1-\zeta)$	f_{cr}/E_c	0.47	1.27%	0.42	3.25%
with shrinkage correction	f_{ct}	f_{cr}/E_c	0.37	0.61%	0.25	3.25%

2.2.4 Tension stiffening mechanism

The exceptional excellent tension stiffening of CA-UHPC compared to NC is attributed to the enhanced post-cracking tensile strength of CA-UHPC as well as the improved interface bond properties between rebar and concrete. On the other hand, the tensile strength of NC suddenly falls to zero the moment reaching the tensile strength f_{ct} due to the brittle fracture under tension. By comparison, the post-cracking residual tensile strength of CA-UHPC only drops from 7.83 MPa to 6.47 MPa [see Fig.2(a) and Table 2] corresponding to the first

cracking to the tensile strain of 0.25%, which is due to the addition of fine steel fibers as well as the improved density by adding fine reactive fillers.

The interface bond properties, which results from chemical adhesion, friction, and mechanical interlocking, shown in Fig.13, ensure the collaborative work of concrete and rebar. Comparison of ultimate bond strength τ_{bm} between different concretes is summarized in Table 6. *fib* Model Code 2010 [32] makes a detailed classification of the bond strength according to the lateral constraint conditions, bond conditions, and failure modes of the pull-out test. Marchand et al.[33] have developed the prediction formula $\tau_{bm}=3.9f_{cm}^{1/2}$ for calculating the ultimate bond strength between rebar and UHPC. Zhao et al.[34] have obtained the ultimate bond strength of 22~33 MPa by conducting pull-out tests for rebars and CA-UHPC, and this study established a similar empirical model $\tau_{bm}=2f_{cm}^{1/2}$ for CA-UHPC based on the test data of Zhao et al[34].

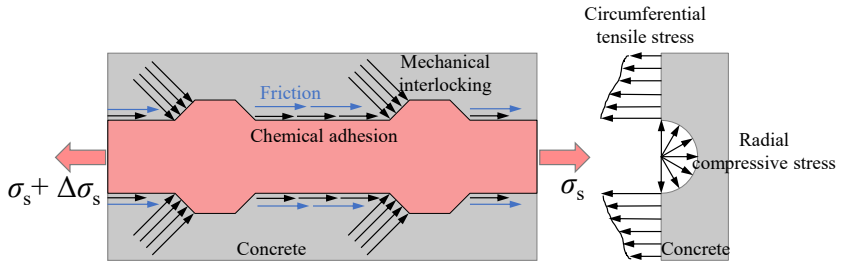

Fig. 13. Interface bond interaction between rebar and concrete.

The most common NC has compressive strength ranging from 38 MPa to 58 MPa, yielding ultimate interface bond strengths of 7.8 MPa to 8.6 MPa according to $\tau_{bm}=7(f_{cm}/25)^{1/4}$ as given in Table 6. The mean compressive strength of CA-UHPC in this study reaches 128 MPa, resulting in ultimate interface bond strength of 22.6 MPa based on $\tau_{bm}=2f_{cm}^{1/2}$. The ultimate bond strength of CA-UHPC is then approximately 3 times higher than NC, which is demonstrating significantly enhanced interface bond properties.

Table 6. Comparison of ultimate bond strength.

Reference	Concrete	V_f	Failure	Bond	τ_{bm}

			modes	condition	
fib MC 2010[32]	NC	0	stirrups, pull-out	Good	$2.5f_{cm}^{1/2}$
				Other	$1.25f_{cm}^{1/2}$
			stirrups, splitting	Good	$8(f_{cm}/25)^{1/4}$
				Other	$5.5(f_{cm}/25)^{1/4}$
			unconfined, splitting	Good	$7(f_{cm}/25)^{1/4}$
				Other	$5(f_{cm}/25)^{1/4}$
Marchand et al.[33]	UHPC	2.5%	pull-out	Good	$3.9f_{cm}^{1/2}$
Zhao et al.[34]	CA-UHPC	2.6%	pull-out	Good	22~33MPa, approximately $2f_{cm}^{1/2}$

Note: V_f denotes fiber volume fraction, f_{cm} is the mean compressive cylinder strength.

3. Tension capacity prediction

The axial tension response of RC members is usually predicted based on the tensile constitutive models of rebar and concrete. Therefore, it is essential to compare the influence of different constitutive models of CA-UHPC, i.e., the tension constitutive model and the tension-stiffening model, on the experimental tensile behavior of R-CA-UHPC. Besides, the restrained shrinkage effect should also be considered in these constitutive models to make a more accurate prediction.

For the convenience of the application, the tension constitutive model of CA-UHPC was further simplified into a tri-linear model based on the energy equivalence principle, shown in Fig.14(b). Moreover, a tensile constitutive model considering the restrained shrinkage effect was also proposed, plotted in Fig.14(c), and denoted as the reduced tri-linear model.

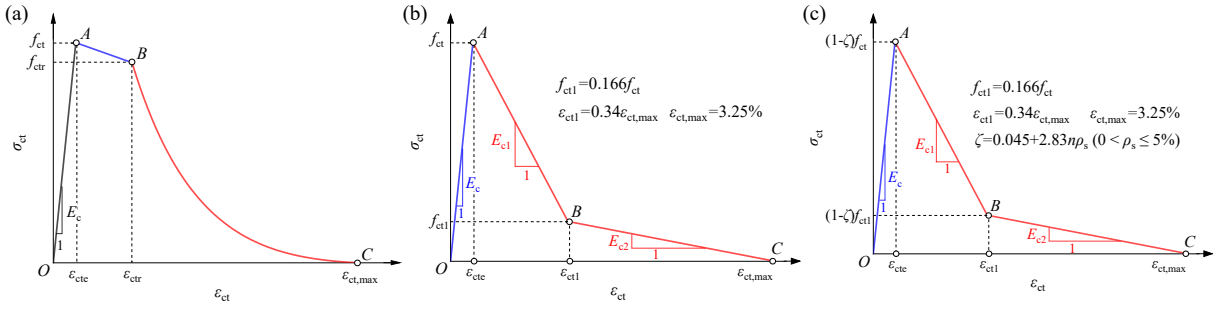

Fig. 14. Tensile constitutive model of CA-UHPC: (a) original model [29]; (b) tri-linear model; and (c) reduced tri-linear model (considering restrained shrinkage effect).

The tri-linear tensile constitutive model of CA-UHPC is expressed as:

$$\sigma_{ct}=\begin{cases}E_c\varepsilon_{ct} & 0\le\varepsilon_{ct}\le\varepsilon_{cte}\\ f_{ct}-E_{c1}\left(\varepsilon_{ct}-\varepsilon_{cte}\right) & \varepsilon_{cte}<\varepsilon_{ct}\le\varepsilon_{ct1}\\ f_{ct1}-E_{c2}\left(\varepsilon_{ct}-\varepsilon_{ct1}\right) & \varepsilon_{ct1}<\varepsilon_{ct}\le\varepsilon_{ct,max}\end{cases} \tag{12}$$

where: f_{ct1}=0.166f_{ct}, ε_{cte}=f_{ct}/E_c, $\varepsilon_{ct,max}$=3.25%, ε_{ct1}=0.34$\varepsilon_{ct,max}$, E_{c1}=(f_{ct}-f_{ct1})/(ε_{ct1}-ε_{cte}), E_{c2}= f_{ct1}/($\varepsilon_{ct,max}$-ε_{ct1}).

The reduced tri-linear tensile constitutive model of CA-UHPC is expressed as:

$$\sigma_{ct}=\begin{cases}E_c\varepsilon_{ct} & 0\le\varepsilon_{ct}\le\varepsilon_{cte}\\ (1-\zeta)f_{ct}-E_{c1}\left(\varepsilon_{ct}-\varepsilon_{cte}\right) & \varepsilon_{cte}<\varepsilon_{ct}\le\varepsilon_{ct1}\\ (1-\zeta)f_{ct1}-E_{c2}\left(\varepsilon_{ct}-\varepsilon_{ct1}\right) & \varepsilon_{ct1}<\varepsilon_{ct}\le\varepsilon_{ct,max}\end{cases} \tag{13}$$

where: f_{ct1}=0.166f_{ct}, ε_{cte} =(1-ζ) f_{ct} /E_c, $\varepsilon_{ct,max}$=3.25%, ε_{ct1}=0.34$\varepsilon_{ct,max}$, E_{c1}=(1-ζ)(f_{ct}-f_{ct1})/(ε_{ct1}-ε_{cte})；E_{c2}=(1-ζ)f_{ct1}/($\varepsilon_{ct,max}$-ε_{ct1}), ζ is the restrained degree and is calculated according to Eq.(11).

The bilinear constitutive model was adopted for the rebar, is shown in Fig.2(c) and expressed as:

$$\sigma_s=\begin{cases}E_s\varepsilon_s & 0\le\varepsilon_s\le\varepsilon_{sy}\\ f_{sy}+E_p\left(\varepsilon_s-\varepsilon_{sy}\right) & \varepsilon_{sy}<\varepsilon_s\le\varepsilon_{su}\end{cases} \tag{14}$$

where the characteristic values are listed in Table 3.

According to the load-sharing approach, the theoretical prediction model for the axial tensile response of R-CA-UHPC during the entire process is given:

$$P=P_{cm}+P_{sm}=A_c\sigma_{ct}+A_s\sigma_s \tag{15}$$

Comparisons between the experimental and the theoretical tensile responses based on the three constitutive models of CA-UHPC, i.e. the tension-stiffening model (TSM), the tension constitutive model (TCM), and the reduced tensile constitutive model (reduced TCM), are shown in Fig.15. Considering that the restrained tensile stress has developed in CA-UHPC

399 before enforcement of external loading, the tension-stiffening model without shrinkage
400 correction was used herein accordingly.

401 It can be observed that the theoretical curves correlate well with the experimental curves
402 on the whole, proving the fine rationality and effectiveness of the three constitutive models of
403 CA-UHPC and the theoretical prediction model for axial tensile response. Specifically, a
404 comparison between the experimental and the theoretical axial loads at four characteristic
405 points, including the first cracking, the yielding, the peak, and one residual points, was
406 conducted, as shown in Fig.16. The first cracking point is related to the service performance,
407 the yielding point corresponds to the ultimate limit state, while the peak point represents the
408 capacity reserve above the yielding. The yielding point is determined by the average member
409 strain reaching the yielding strain of the rebar. Moreover, the distinguished feature of
410 CA-UHPC compared with NC is the excellent toughness owing to the fiber/matrix debonding
411 at the tension softening stage. Therefore, the design of CA-UHPC structures should be
412 distinguished from the conventional RC structures, especially for structures under accidental
413 actions, including earthquakes, impacts and explosions, to fully utilize the high
414 energy-dissipating capacity. Hence, the residual point, which is captured by the achievement
415 of 10 times the yielding strain (close to the end of the yielding platform of rebar), has been
416 also chosen for the analysis.

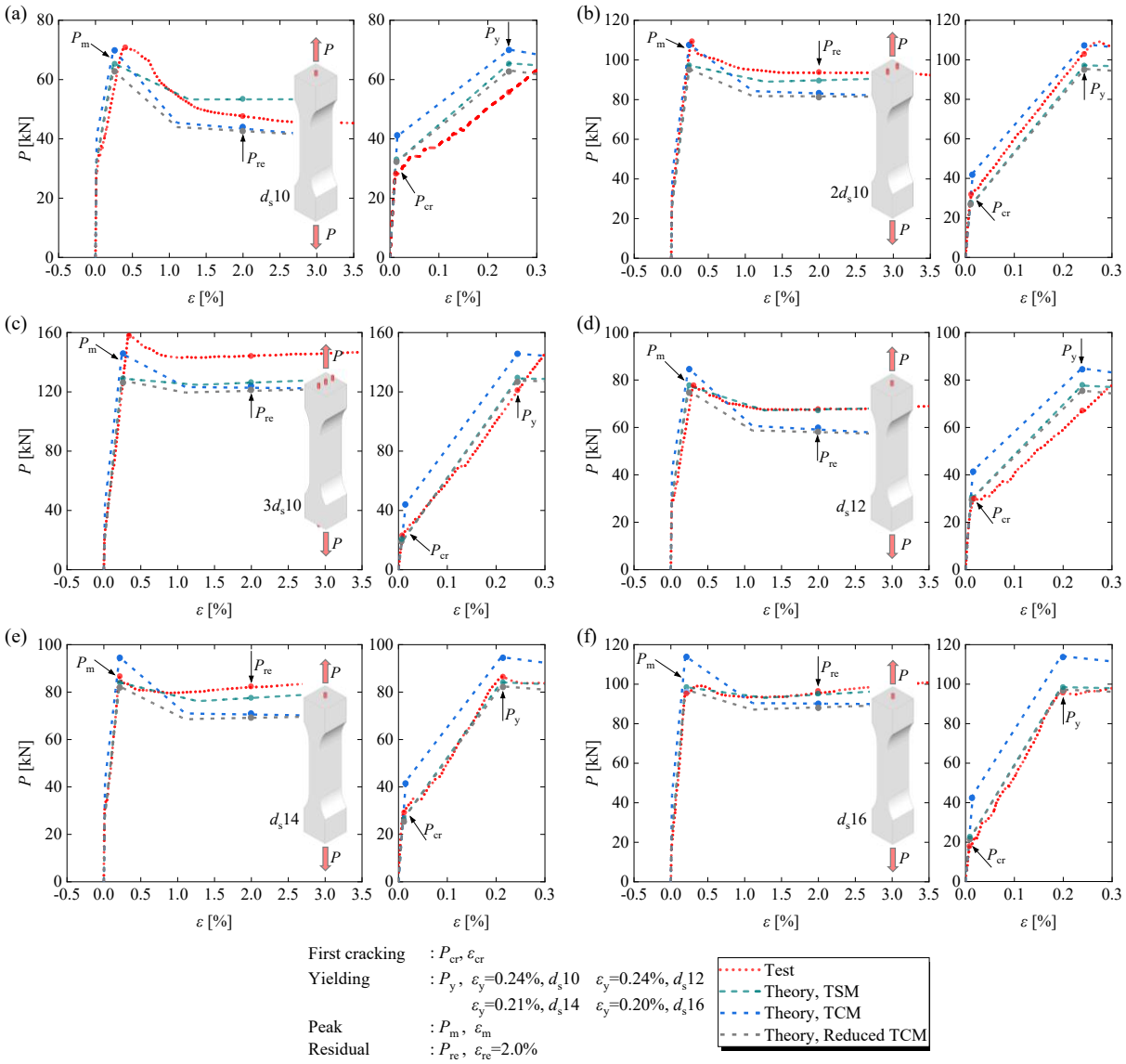

Fig. 15. Comparisons between theoretical and experimental member responses: (a) d_s10; (b) $2d_s10$; (c) $3d_s10$; (d) d_s12; (e) d_s14; and (f) d_s16.

As compared, for the first cracking load P_{cr}, the prediction values of the tension-stiffening model and the reduced tension constitutive model are 1.03 times the experimental value with a coefficient of variation of 14%, which exhibits higher estimating accuracy than the tensile constitutive model. For the yielding load P_y, the tension-stiffening model and the reduced tension constitutive model present a deviation between the predicted value and the experimental value within 5%, while that of the tension constitutive model exceeds 15%. The tension constitutive model substantially overestimates both P_{cr} and P_y.

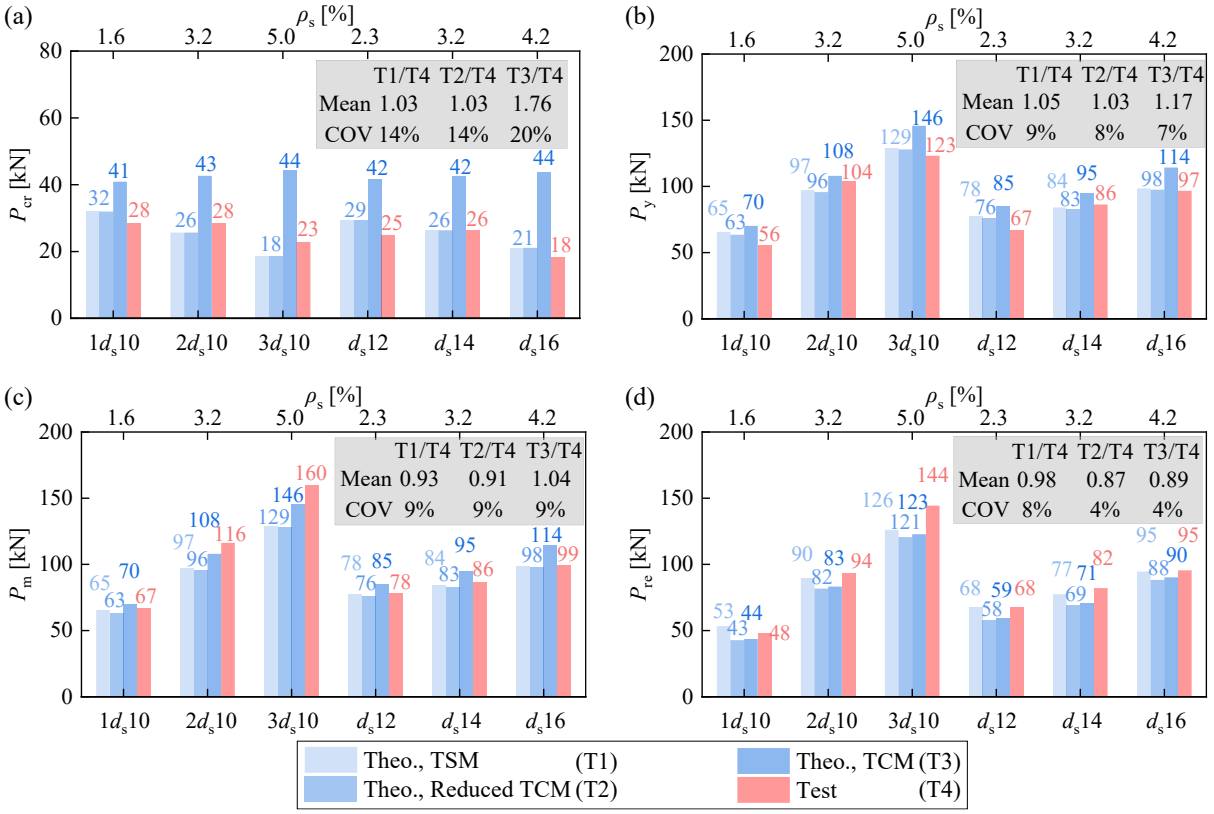

Fig. 16. Comparison between theoretical and experimental characterized loads: (a) first cracking load P_{cr}; (b) yielding load P_y; (c) peak load P_m; and (d) residual load P_{re}.

For the peak load P_m, the tension-stiffening model and the reduced tension constitutive model underestimate the value while the tension constitutive model overestimates, but the prediction accuracies are all within 10% a coefficient of variation of 9%. For the residual load P_{re}, the two tensile constitutive models underestimate the value with deviations of 11% and 13%, while the tension-stiffening model makes the best prediction with an accuracy up to 98%. This is caused by the difference in constitutive mechanism between strain softening and tension stiffening.

To sum up, for the prediction of P_{cr} and P_y it is suggested using the tension-stiffening model or the reduced tension constitutive model, whereas for the prediction of P_m each one of the three constitutive models can be adopted, and the prediction of P_{re} is recommended to be performed through the tension-stiffening model. Moreover, the proposed tension-stiffening model of CA-UHPC has been demonstrated to provide accurate estimations for all the

442 characteristic loads for R-CA-UHPC under axial tension.

443 **4. Crack width calculation**

444 *4.1 Calculation principles*

445 The cracking stage of R-CA-UHPC or R-UHPC members is similar to that of normal RC
446 members, which is often divided into the crack formation stage and stabilized cracking stage.
447 Tan et al. [35] and Terjesen et al. [36] proposed analytical models for crack width calculation
448 for normal RC members, including separate solutions for the two stages. While most
449 regulations and guidelines do not clearly differentiate between the two stages. For
450 R-CA-UHPC, there is a smooth transition between the uncracked and cracked stages as
451 shown in Fig.7, and it is therefore unnecessary to distinguish between the two stages. This
452 research applies three different approaches for normal RC structures [37–39] to R-UHPC
453 structural members, considering only the stabilized cracking stage, including also the tension
454 stiffening effect.

455 For the uniaxial tension RC member shown in Fig.17, assuming that the average crack
456 spacing l_m (for the stabilized cracking stage) is known, the average crack width w_m
457 continuously develops with the increase of external load after the first cracking. Neglecting
458 the change in tension stiffening, the elongation of concrete within l_m is mainly due to the
459 increase in the average crack width w_m. In other words, the average crack width is the amount
460 of elongation of concrete that occurs after cracking to maintain deformation compatibility
461 with the rebar, and can be expressed as:

462
$$w_m = \Delta l_m - \Delta l_{me} \tag{16}$$

463 where Δl_m is the average elongation within l_m; and Δl_{me} is the average elongation at first
464 cracking.

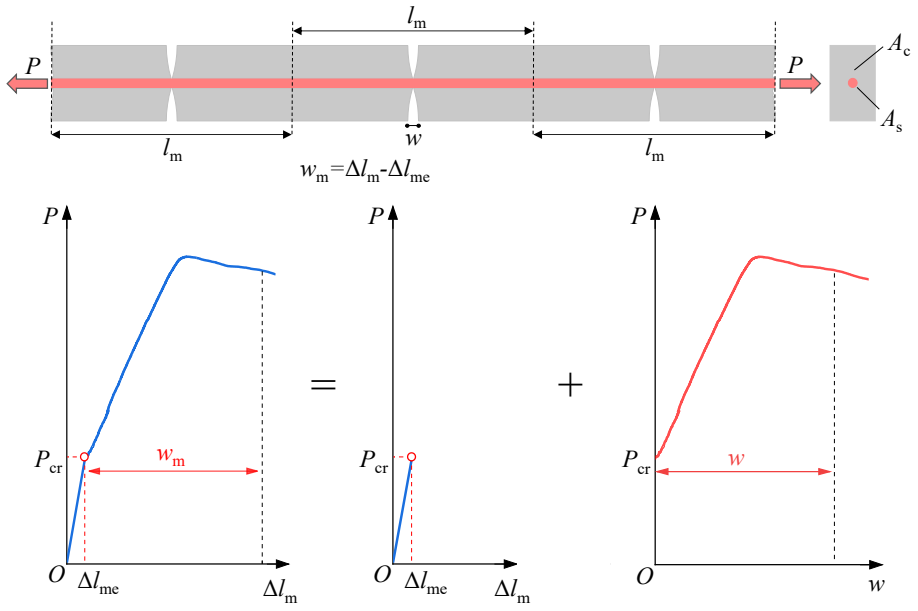

Fig. 17. Principle of tension-stiffening-based crack width calculation.

According to the relationship between elongation and nominal strain, Eq.(16) can be further developed to:

$$w_m = l_m\left(\varepsilon_m - \varepsilon_{me}\right) \tag{17}$$

where ε_m is the average member strain within l_m; and ε_{me} is the elastic limit strain or the concrete strain at the first cracking.

It is generally assumed that the average member strain ε_m equals the average rebar strain ε_{sm} to investigate the axial tension behavior of RC members, thus giving:

$$\varepsilon_m = \varepsilon_{sm} \tag{18}$$

Substituting Eq.(18) into Eq.(1), gives:

$$\varepsilon_m = \varepsilon_s - \Delta\varepsilon_s \tag{19}$$

Based on the equivalent relationship of tension stiffening, i.e., Eq.(6), the following equation is obtained:

$$\Delta\varepsilon_s = \frac{\beta A_c f_{cr}}{E_s A_s} = \frac{\beta f_{cr}}{E_s \rho_s} \tag{20}$$

Substituting Eq.(20) into Eq.(19), gives:

$$\varepsilon_{\mathrm{m}} = \varepsilon_{\mathrm{s}} - \Delta\varepsilon_{\mathrm{s}} = \frac{\sigma_{\mathrm{s}}}{E_{\mathrm{s}}} - \frac{\beta f_{\mathrm{cr}}}{E_{\mathrm{s}}\rho_{\mathrm{s}}} = \frac{1}{E_{\mathrm{s}}}\left(\sigma_{\mathrm{s}} - \frac{\beta f_{\mathrm{cr}}}{\rho_{\mathrm{s}}}\right) \tag{21}$$

The first cracking strain $\varepsilon_{\mathrm{me}}$ can be expressed as:

$$\varepsilon_{\mathrm{me}} = \frac{f_{\mathrm{cr}}}{E_{\mathrm{c}}} \tag{22}$$

Finally, the average crack width w_{m} can be obtained by substituting Eq.(21) and Eq.(22) into Eq.(17),and is now expressed as:

$$w_{\mathrm{m}} = l_{\mathrm{m}}\left[\frac{1}{E_{\mathrm{s}}}\left(\sigma_{\mathrm{s}} - \frac{\beta f_{\mathrm{cr}}}{\rho_{\mathrm{s}}}\right) - \frac{f_{\mathrm{cr}}}{E_{\mathrm{c}}}\right] \tag{23}$$

where σ_{s} is the tensile stress of the bare rebar, without the tensile contribution of the concrete; β is the bond factor, which can be simplified as a constant and be taken as 0.8 for UHPC according to Fig.11(b); ρ_{s} is the reinforcement ratio; f_{cr} is the first cracking strength considering the restrained shrinkage effect, which can be predicted according to Eq.(10) and (11).

The proposed method of crack width prediction for R-UHPC members is based on the tension stiffening effect, and is thereby named the tension-stiffening method (TSM).

4.2 Model parameters for members exposed to flexure

For the crack width calculation, which is expressed in Eq.(24), the reinforcement ratio ρ_{s} should be calculated as the effective reinforcement ratio $\rho_{\mathrm{s,eff}}$ based on the effective tension area of concrete $A_{\mathrm{c,eff}}$ (see Fig.18). It should be noted that the average crack width obtained according to Eq.(24) is at the center of gravity of the rebar, therefore the average crack width w_{cm} at the tensile edge of structural element should be amplified according to the geometric relationship, as expressed in Eq.(25) and shown in Fig.18:

$$w_{\mathrm{m}} = l_{\mathrm{m}}\left[\frac{1}{E_{\mathrm{s}}}\left(\sigma_{\mathrm{s}} - \frac{\beta f_{\mathrm{cr}}}{\rho_{\mathrm{s,eff}}}\right) - \frac{f_{\mathrm{cr}}}{E_{\mathrm{c}}}\right] \tag{24}$$

$$w_{\mathrm{cm}} = \frac{y}{y - a_{\mathrm{s}}} w_{\mathrm{m}} \tag{25}$$

where a_s is the distance between the center of gravity of rebar and the tensile edge of the structural element, and y is taken as the distance between the neutral axis of the uncracked composite section and the tensile edge of the structural element considering the design safety.

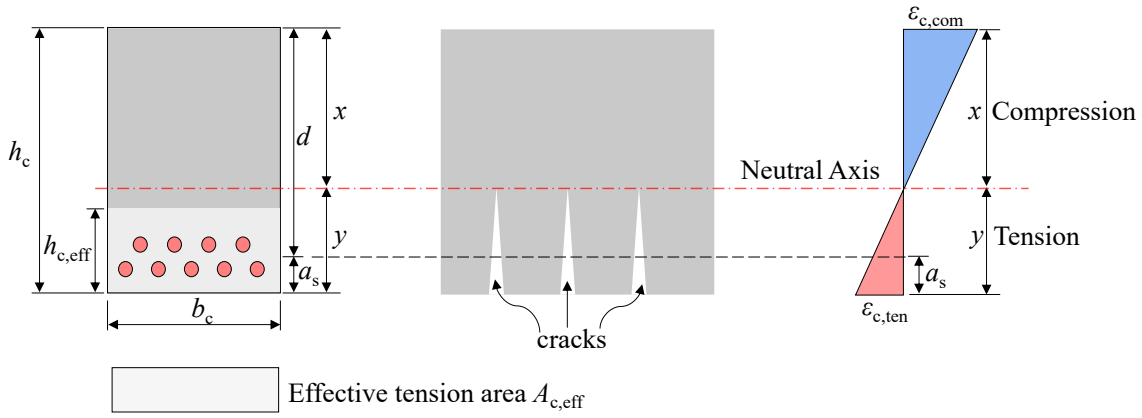

Fig. 18. Schematic diagram of effective tension area of concrete and amplification factor.

Moreover, the maximum crack width w_{max} at the tensile edge of the structural element is developed by including the short-term amplification factor τ_s and the long-term amplification factor τ_l, as given in Eq.(26):

$$w_{max} = \tau_l \tau_s w_{cm} = \tau_l \tau_s \frac{y}{y - a_s} l_m \left[\frac{1}{E_s} \left(\sigma_s - \frac{\beta f_{cr}}{\rho_{s,eff}} \right) - \frac{f_{cr}}{E_c} \right] \tag{26}$$

where the amplification factors according to the Chinese design code GB50010-2010 [39], are τ_l taken as 1.5, and τ_s taken as 1.9 for axial tension members and eccentric tension members, and 1.66 for flexural tension members.

There are three parameters in Eq.(26) that need to be quantified for crack width prediction, the effective tension area of concrete $A_{c,eff}$ (corresponding to the effective reinforcement ratio $\rho_{s,eff}$), the average crack spacing l_m, and the tensile stress σ_s of the bare rebar.

(I) Effective tension area $A_{c,eff}$

The effective tension area of UHPC illustrated in Fig.18 was calculated using three methods, method 1 (M1), method 2 (M2), and method 3 (M3), which were referred to

GB50010-2010 [39], ACI 318-14[38], and Eurocode 2[37], respectively. The corresponding values for the effective tension zone $h_{c,eff}$ are listed in Table 7.

Table 7. Effective tension depth $h_{c,eff}$ of UHPC.

M1: GB50010-2010	$0.5h_c$
M2: ACI 318-14	$2a_s$
M3: Eurocode 2	$\min\{2.5(h_c\text{-}d), (h_c\text{-}x)/3, h_c/2\}$

Note: h_c is the depth of the R-UHPC beams or slabs.

(II) Average crack spacing l_m

When the effective tension area is calculated based on M1, the average crack spacing l_m is determined by the formula in GB50010-2010 [39] as:

$$l_m = \alpha_f \left(1.9c + 0.08 \frac{d_s}{\rho_{s,eff}} \right) \tag{27}$$

where α_f is the correction coefficient for the effect of steel fibers; c is the concrete cover to the longitudinal rebar; and d_s is the rebar diameter, according to the Eurocode 2[37], where several rebar diameters are used in a section, an equivalent diameter should be used.

When adopting M2 or M3, the average crack spacing l_m is given by Eq.(28):

$$l_m = k_1 c + k_2 \frac{d_s}{\rho_{s,eff}} \tag{28}$$

where k_1 and k_2 are model parameters to be fitted.

The measured average crack spacing for R-UHPC beams and slabs in existing literature[40,41] are summarized in Table 8 together with the geometry parameters of the specimens. The screening criteria for selecting the literature are: (1) The volume fraction of steel fibers in UHPC is in the range 1.5%~3.5%; (2) UHPC exhibits multiple cracking characteristics; (3) The specimens are reinforced with steel rebars with ribs without prestressing. Based on these test data, the fitted results of unknown parameters in Eq.(27) and Eq.(28) are listed in Table 9. The fitted k_1 values for M2 and M3 are 1.77 and 1.71, respectively, both significantly lower than the value of 3.4 recommended by Eurocode 2.

Similarly, the fitted k_2 values for M2 and M3 are 0.09 and 0.07, respectively, which also fall below the recommended value of 0.17.

Table 8. Experimental average crack spacing parameters for R-UHPC beams and slabs.

Ref.	No.	h_c [mm]	b_c [mm]	d_s [mm]	A_s [mm^2]	c [mm]	a_s [mm]	l_m [mm]
[40]	B-3	160	350	20	1257	20	30	58.18
	B-4	160	350	20	1257	20	30	57.26
	C-1	160	350	16	1206	20	28	50.48
	C-4	160	350	16	1206	20	28	55.46
	D-1	160	350	18	1018	20	29	62.76
	E-1	160	350	22	1521	20	31	55.62
[41]	B20R1	300	150	16	402	26	34	105.00
	B20R3	300	150	22	1140	26	38	73.00
	B20R5	300	150	24	1742	26	60	63.00
	B20R7	300	150	28	2463	26	68	66.00
	B30R1	300	150	16	402	26	34	92.00
	B30R3	300	150	22	1140	26	38	68.00
	B30R5	300	150	24	1742	26	60	65.00
	B30R7	300	150	28	2463	26	68	61.00

Table 9. Fitted parameters of mean crack spacing l_m.

M1, Eq.(27)	M2, Eq.(28)		M3, Eq.(28)	
α_f	k_1	k_2	k_1	k_2
0.83	1.71	0.09	1.77	0.07

(III) Rebar stress σ_s

According to the tension-stiffening calculation principle, σ_s is the stress of the bare rebar under any external load P. For R-UHPC beams and slabs, the calculation method referred to GB50010-2010[39], is given in Eq.(29):

$$\sigma_s = \frac{M}{0.87 d A_s} \tag{29}$$

where M is the bending moment; A_s is the area of rebar in tension; and d is the vertical distance from the center of gravity of the tension rebars to the compressive edge of concrete, as shown in Fig.18.

4.3 Calculation method validation

4.3.1 Axial tension members

The axial tension test results for R-CA-UHPC members were used to validate the quality

of the tension-stiffening method (TSM) for crack width calculation. Results are compared in Fig.19, where the experimental values of the crack widths were captured from the main cracks by a crack observation instrument with an accuracy of 0.01 mm, while the TSM values were developed by processing the measured axial load-elongation curves based on Eq.(16).

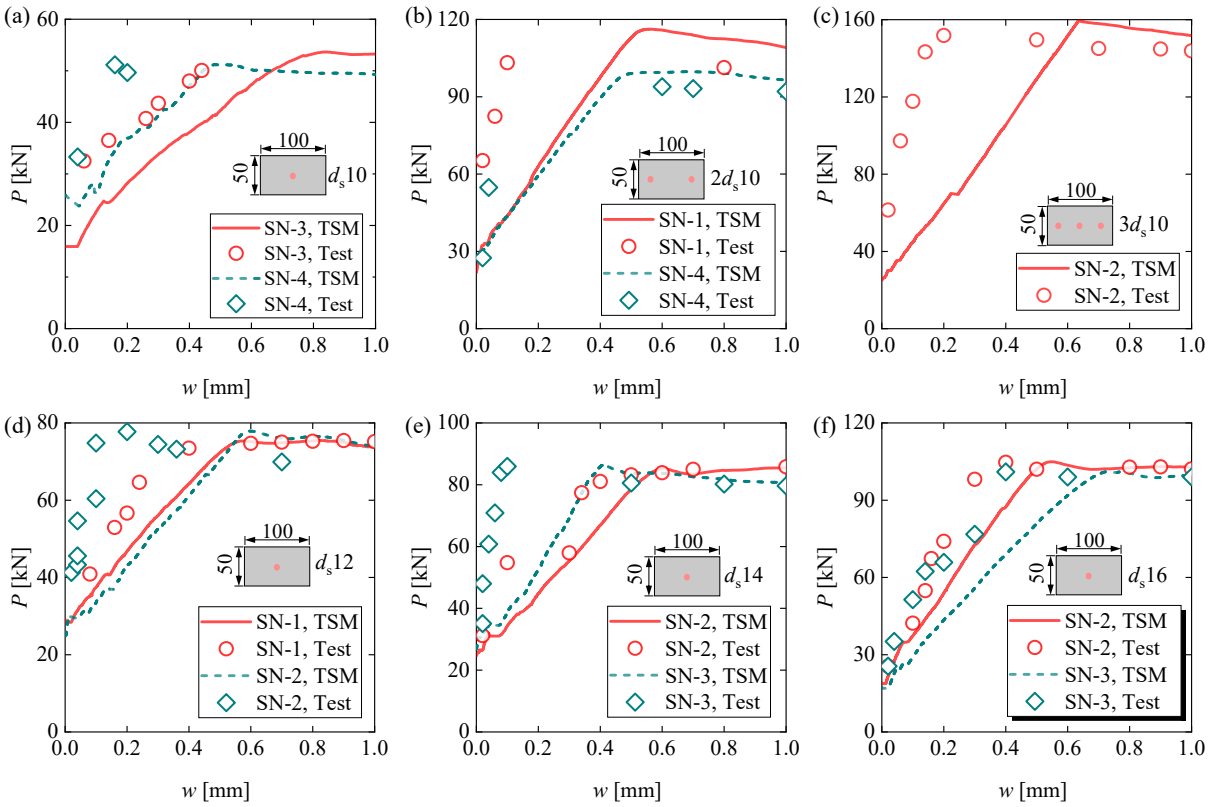

Fig. 19. Comparison between theoretical and test crack widths of R-CA-UHPC members: (a) d_s10; (b) 2d_s10; (c) 3d_s10; (d) d_s12; (e) d_s14; and (f) d_s16.

It is observed that the experimental values are smaller than the TSM values before reaching the peak load (close to the yielding load). This is because the CA-UHPC presents multiple cracks at the pre-yielding stage. The TSM values are the sum of crack widths of all the cracks over the gauge length of 200 mm, while the experimental values are for one crack. The test values show good agreement with the TSM values at the post-peak stage. This could be interpreted by the emergence and development of localized cracking, and both the test values and the TSM values represent the localized cracks. Overall, the test values are in good agreement with the TSM values, verifying the rationality of the calculation principle of the

TSM.

4.3.2 Flexural tension members

The measured maximum crack widths of R-UHPC beams and slabs in some experimental studies [40–43] were compared with the calculated values from the proposed TSM, as shown in Fig.20, where TSM-1/2/3 denote M1, M2, and M3 for calculating the effective tension area of concrete, respectively. In general, the proposed TSM overestimates the maximum crack widths of the R-UHPC beams and slabs, except for specimen C2 in Wang's slab tests[40].

The overall comparison between the TSM and the experimental values for all specimens in each reference is shown in Fig.21. The ratios of TSM-1 to test, TSM-2 to test, and TSM-3 to test, range from 1.09 to 1.68, 1.49 to 2.59, and 1.32 to 2.11, respectively. TSM-1 is demonstrated to have the best prediction accuracy. Considering the induced difficulty in determining the main cracks and the related crack widths by incorporating steel fibers for UHPC, the TSM is proven to effectively calculate the maximum crack width for R-UHPC flexural tension members. Moreover, method 1 is suggested to be applied in determining the effective tension area of UHPC elements.

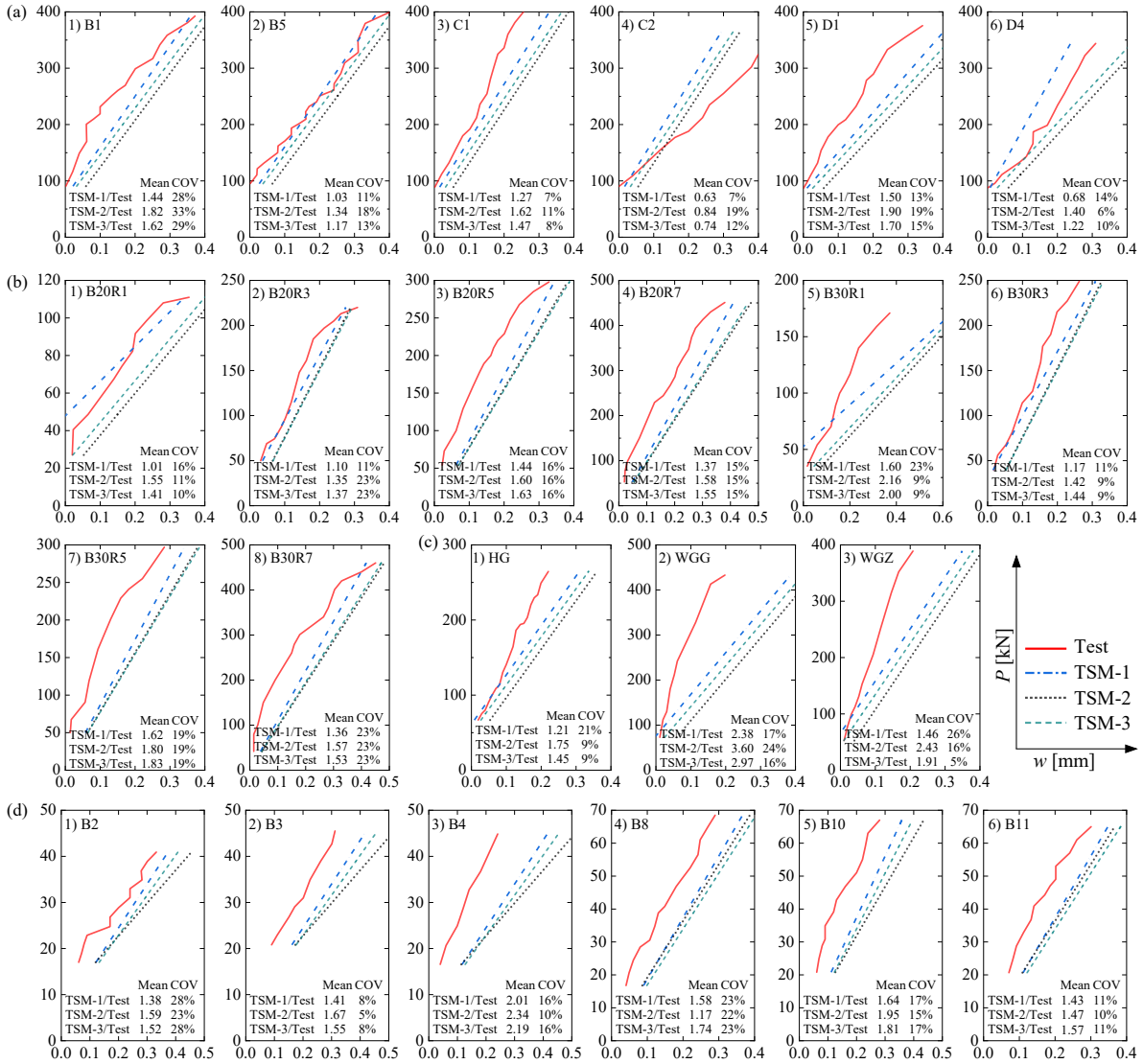

Fig. 20. Comparison between the TSM and the experimental maximum crack widths of R-UHPC beams and slabs: (a) Wang [40]; (b) Feng et al.[41]; (c) Wang [42]; and (d) Li [43].

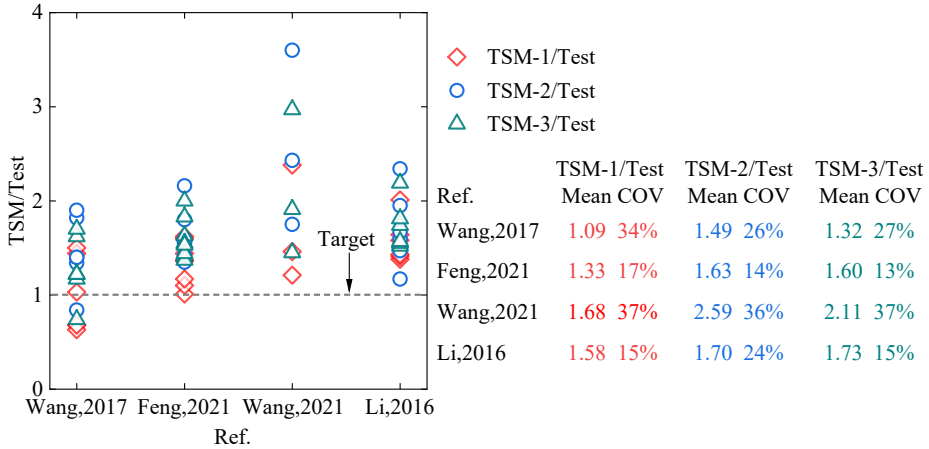

Ref.	TSM-1/Test Mean	COV	TSM-2/Test Mean	COV	TSM-3/Test Mean	COV
Wang,2017	1.09	34%	1.49	26%	1.32	27%
Feng,2021	1.33	17%	1.63	14%	1.60	13%
Wang,2021	1.68	37%	2.59	36%	2.11	37%
Li,2016	1.58	15%	1.70	24%	1.73	15%

Fig. 21. Overall comparison between the TSM and the test values.

5. Conclusions

Due to the need for SLS and ULS design guidelines for CA-UHPC structures, experimental and theoretical research have been carried out. Based on the reported experimental studies on the uniaxial tension behavior of R-CA-UHPC members, this study aims to identify the tension stiffening effect. The influence of restrained shrinkage was clarified, and the tension stiffening model was developed. In addition, a tension-stiffening-based crack width calculation method was proposed and validated. Based on the above investigations, the main conclusions are:

(1) CA-UHPC exhibits superior tension stiffening compared to normal concrete, with its tension-stiffening bond factor of 0.81 at rebar yielding being approximately triple that of normal concrete.

(2) The restrained effect of rebars on UHPC shrinkage significantly influences tension stiffening of R-CA-UHPC before rebar yielding, but becomes negligible afterwards. This difference can be attributed to the pronounced fiber pull-out behavior across cracks at the point of rebar yielding, causing crack localization.

(3) A tension-stiffening model for cracked R-CA-UHPC was developed and presented with and without shrinkage correction. The effect of shrinkage correction was proven to be independent of the reinforcement ratios. The proposed tension-stiffening model exhibited better accuracy in predicting the tensile response of R-CA-UHPC members compared to the tensile constitutive model of CA-UHPC.

(4) A tension-stiffening-based approach was developed for calculating crack widths of R-UHPC members by assuming the deformation compatibility between concrete and rebar. Methods to calculate the two decisive parameters, the effective tension area and average crack spacing, were discussed and quantitatively determined. The proposed approach was proven to be effective in predicting the crack widths in

R-UHPC members under both axial and flexural loading.

Data availability statement

Some or all data, models, or code that support the findings of this study are available from the corresponding author upon reasonable request.

Acknowledgements

The financial support provided by Fujian Transportation Science and Technology Project (Grant No.202126) is greatly appreciated by the authors. Zhanchong Shi also acknowledges the EU-funded MSCA Postdoctoral Fellowship (Grant No. 101149607).

References

[1] Collins MP, Mitchell D. Prestressed concrete structures. Prentice Hall Englewood Cliffs, NJ; 1991.

[2] Abrishami HH, Mitchell D. Influence of steel fibers on tension stiffening. ACI Structural Journal 1997;94:769–75.

[3] Bischoff PH. Tension stiffening and cracking of steel fiber-reinforced concrete. Journal of Materials in Civil Engineering 2003;15:174–82.

[4] Lee S-C, Cho J-Y, Vecchio FJ. Tension-Stiffening Model for Steel Fiber-Reinforced Concrete Containing Conventional Reinforcement. ACI Structural Journal 2013;110.

[5] Moreno DM, Trono W, Jen G, Ostertag C, Billington SL. Tension stiffening in reinforced high performance fiber reinforced cement-based composites. Cement and Concrete Composites 2014;50:36–46.

[6] Soltani M, An X, Maekawa K. Computational model for post cracking analysis of RC membrane elements based on local stress–strain characteristics. Engineering Structures 2003;25:993–1007.

[7] Kwak H-G, Kim D-Y. Material nonlinear analysis of RC shear walls subject to

monotonic loadings. Engineering Structures 2004;26:1517–33.

[8] Stramandinoli RS, La Rovere HL. An efficient tension-stiffening model for nonlinear analysis of reinforced concrete members. Engineering Structures 2008;30:2069–80.

[9] Graybeal B, Brühwiler E, Kim B-S, Toutlemonde F, Voo YL, Zaghi A. International perspective on UHPC in bridge engineering. Journal of Bridge Engineering 2020;25:04020094.

[10] Yoo D-Y, Kim S, Kim M-J. Comparative shrinkage behavior of ultra-high-performance fiber-reinforced concrete under ambient and heat curing conditions. Construction and Building Materials 2018;162:406–19. https://doi.org/10.1016/j.conbuildmat.2017.12.029.

[11] Yang L, Shi C, Wu Z. Mitigation techniques for autogenous shrinkage of ultra-high-performance concrete–A review. Composites Part B: Engineering 2019;178:107456.

[12] Wang Y, Shao X, Cao J. Experimental study on basic performances of reinforced UHPC bridge deck with coarse aggregates. Journal of Bridge Engineering 2019;24:04019119.

[13] Yuan H. Theoretical analysis and experimental research on tensile performance of reinforced reactive powder concrete. Doctoral thesis. Beijing Jiaotong University, 2009.

[14] Sturm A, Visintin P, Oehlers D, Seracino R. Time-dependent tension-stiffening mechanics of fiber-reinforced and ultra-high-performance fiber-reinforced concrete. Journal of Structural Engineering 2018;144:04018122.

[15] Hung C-C, Lee H-S, Chan SN. Tension-stiffening effect in steel-reinforced UHPC composites: Constitutive model and effects of steel fibers, loading patterns, and rebar sizes. Composites Part B: Engineering 2019;158:269–78. https://doi.org/10.1016/j.compositesb.2018.09.091.

[16] Bian C, Wang J-Y. Mechanical and damage mechanisms of reinforced ultra high performance concrete under tensile loading. Construction and Building Materials

671 2019;226:259–79. https://doi.org/10.1016/j.conbuildmat.2019.07.162.
672 [17] Bian C, Guo J, Wang J, Xiao J. Nominal tensile strength reduction and its mechanism of
673 ultra-high performance concrete with steel bar reinforcements. Journal of Building
674 Engineering 2023;65:105778.
675 [18] Zhang Z, Shao X-D, Zhu P. Direct tensile behaviors of steel-bar reinforced ultra-high
676 performance fiber reinforced concrete: Effects of steel fibers and steel rebars.
677 Construction and Building Materials 2020;243:118054.
678 [19] Qiu M, Zhang Y, Qu S, Zhu Y, Shao X. Effect of reinforcement ratio, fiber orientation,
679 and fiber chemical treatment on the direct tension behavior of rebar-reinforced UHPC.
680 Construction and Building Materials 2020;256:119311.
681 https://doi.org/10.1016/j.conbuildmat.2020.119311.
682 [20] Khorami M, Navarro-Gregori J, Serna P. Tensile behaviour of reinforced UHPFRC
683 elements under serviceability conditions. Materials and Structures 2021;54:1–17.
684 [21] Fields K, Bischoff PH. Tension stiffening and cracking of high-strength reinforced
685 concrete tension members. ACI Structural Journal 2004;101:447–56.
686 [22] Weiss WJ, Yang W, Shah SP. Shrinkage cracking of restrained concrete slabs. Journal of
687 Engineering Mechanics 1998;124:765–74.
688 [23] AFNOR. NF P 18-710 National addition to Eurocode 2 —Design of Concretestructures:
689 specific rules for Ultra-High Performance Fibre-Reinforced Concrete(UHPFRC). France:
690 2016.
691 [24] JSCE F. Recommendations for design and construction of ultra-high strength fiber
692 reinforced concrete structures (Draft). Tokyo, Japan: Japan Society of Civil Engineers;
693 2004.
694 [25] Leutbecher T, Fehling E. Tensile behavior of ultra-high-performance concrete reinforced
695 with reinforcing bars and fibers: minimizing fiber content. ACI Structural Journal

2012;109:253.

[26] Luo J, Shao X, Fan W, Cao J, Deng S. Flexural cracking behavior and crack width predictions of composite (steel+ UHPC) lightweight deck system. Engineering Structures 2019;194:120–37.

[27] Qiu M. Study on the basic performance and calculation theory of reinforced UHPC members. Doctoral thesis. Hunan University, 2021.

[28] Shi Z, Liang M, Su Q, Kanstad T, Ferrara L. Tensile behavior of rebar-reinforced coarse aggregate ultra-high performance concrete (R-CA-UHPC) members: Experiments and restrained shrinkage creep effect. Cement and Concrete Composites 2024;151:105574. https://doi.org/10.1016/j.cemconcomp.2024.105574.

[29] Shi Z, Su Q, Kavoura F, Veljkovic M. Uniaxial tensile response and tensile constitutive model of ultra-high performance concrete containing coarse aggregate (CA-UHPC). Cement and Concrete Composites 2023;136:104878. https://doi.org/10.1016/j.cemconcomp.2022.104878.

[30] Bischoff PH. Effects of shrinkage on tension stiffening and cracking in reinforced concrete. Canadian Journal of Civil Engineering 2001;28:363–74.

[31] Yoo D-Y, Banthia N, Yoon Y-S. Effectiveness of shrinkage-reducing admixture in reducing autogenous shrinkage stress of ultra-high-performance fiber-reinforced concrete. Cement and Concrete Composites 2015;64:27–36.

[32] International Federation for Structural Concrete. fib Model Code for Concrete Structures 2010. Lausanne, Switzerland: 2013.

[33] Marchand P, Baby F, Khadour A, Battesti T, Rivillon P, Quiertant M, et al. Bond behaviour of reinforcing bars in UHPFRC: Experimental investigation. Mater Struct 2016;49:1979–95. https://doi.org/10.1617/s11527-015-0628-0.

[34] Zhao C, Li H, Deng K. Experimental study on bonding performance between rebar and

721 coarse aggregate ultra-high performance concrete. Journal of Southwest Jiaotong
722 University 2019;54:937–44.
723 [35] Tan R, Hendriks MA, Geiker M, Kanstad T. Analytical calculation model for predicting
724 cracking behavior of reinforced concrete ties. Journal of Structural Engineering
725 2020;146:04019206.
726 [36] Terjesen O, Kanstad T, Tan R. Simplified modified tension chord model: An alternative
727 crack width calculation model to Eurocode 2 and fib model codes. Structural Concrete
728 2024;25:4586–608.
729 [37] European Committee for Standardization. EN 1992-1-1: Eurocode 2: Design of concrete
730 structures - Part 1-1: General rules and rules for buildings. Brussels, Belgium: 2004.
731 [38] American Concrete Institute. ACI 318-14 Building Code Requirements for Structural
732 Concrete. Farmington Hills, the USA: 2014.
733 [39] Ministry of Housing and Urban Rural Development of the People's Republic of China.
734 GB 50010-2010 Code for design of concrete structures. Beijing, China: China
735 Architecture & Building Press; 2011.
736 [40] Wang C. Experimental research on flexural behavior of ultra-high performance concrete
737 structure. Master's dissertation. Southwest Jiaotong University, 2017.
738 [41] Feng Z, Li C, Yoo D-Y, Pan R, He J, Ke L. Flexural and cracking behaviors of reinforced
739 UHPC beams with various reinforcement ratios and fiber contents. Engineering
740 Structures 2021;248:113266. https://doi.org/10.1016/j.engstruct.2021.113266.
741 [42] Wang Y. Research on flexural performance of ultra-high performance concrete
742 lightweight bridge structure. Doctoral thesis. Hunan University, 2021.
743 [43] Li L. Experimental research on flexural behavior of reactive powder concrete structure.
744 Master's dissertation. Southwest Jiaotong University, 2016.
745